The midbody interactome reveals new unexpected roles for PP1 phosphatases in cytokinesis

Luisa Capalbo[1], Zuni I. Bassi[1], Marco Geymonat[2], Sofia Todesca[1], Liviu Copoiu[1†], Anton Enright[1], Giuliano Callaini[3], Maria Giovanna Riparbelli[4], Lu Yu[5≠], Jyoti Choudhary[5≠], Enrico Ferrero[2,6#], Sally Wheatley[7], Max E. Douglas[8‡], Masanori Mishima[8,9] and Pier Paolo D'Avino[1*]

[1]Department of Pathology, University of Cambridge, Tennis Court Road, Cambridge, CB2 1QP, UK

[2]Department of Genetics, University of Cambridge, Downing Street, Cambridge, CB2 3EH, UK

[3]Department of Medical Biotechnologies and [4]Department of Life Sciences, University of Siena, Via A. Moro 4, 53100 Siena, Italy

[5]The Wellcome Trust Sanger Institute, Wellcome Genome Campus, Hinxton, CB10 1SA, UK

[6]Cambridge Systems Biology Centre, University of Cambridge, Tennis Court Road, Cambridge, CB2 1QR, UK

[7]School of Life Sciences, University of Nottingham, Nottingham, NG7 2UH, UK

[8]Wellcome Trust/Cancer Research UK Gurdon Institute, Cambridge CB2 1QN, UK

[9]Centre for Mechanochemical Cell Biology and Division of Biomedical Sciences, Warwick Medical School, University of Warwick, Coventry, CV4 7AL, UK.

*Correspondence to:

Pier Paolo D'Avino, email: ppd21@cam.ac.uk

†Present address: Department of Biochemistry, University of Cambridge, UK

≠ Present address: The Institute of Cancer Research, 123 Old Brompton Road, London SW7 3RP, UK

Present address: Autoimmunity, Transplantation and Inflammation Bioninfomatics, Novartis Institutes for BioMedical Research, 4056 Basel, Switzerland

‡ Present address: Chromosome Replication Laboratory, The Francis Crick Institute, 1 Midland Road, London NW1 1AT, UK

Abstract

The midbody is an organelle assembled at the intercellular bridge that connects the two daughter cells at the end of mitosis. It is composed of a multitude of proteins, organized in a precise and stereotyped pattern, that control the final separation of the daughter cells and prevent incorrect genome segregation. Furthermore, recent evidence indicates that the midbody is involved in many other important processes, including cell fate, pluripotency, apical-basal polarity, tissue organization, and cilium and lumen formation. Understanding the regulation and interactions of midbody proteins is therefore essential to unravel how this organelle executes its multiple functions. Here, we report the first experimentally-based characterization of the intricate midbody protein-protein interaction network (interactome), which identifies a plethora of novel interactions and provides an extremely valuable resource for dissecting the multiple roles of the midbody. Initial analysis of this interactome already revealed that PP1β-MYPT1 phosphatase regulates microtubule dynamics in late cytokinesis and de-phosphorylates the kinesin component MKLP1/KIF23 of the centralspindlin complex, a key cytokinesis regulator. This de-phosphorylation antagonizes Aurora B kinase in order to modify the functions of centralspindlin and its interactions in late cytokinesis. Our findings expand the repertoire of PP1 functions during mitosis and indicate that spatiotemporal changes in the distribution of kinases and counteracting phosphatases finely tune the activity of cytokinesis proteins.

Introduction

Growth, development and reproduction in multicellular organisms depend on the faithful segregation of genomic and cytoplasmic material that occur during cell division. Errors during this process are responsible for many human diseases, including cancer. In the final step of cell division, the mother cell divides into two daughter cells during the process of cytokinesis. This major cell shape change requires the assembly and coordinated activity of two cytoskeletal structures: the actomyosin contractile ring, which assembles at the equatorial cortex and drives the ingression of the cleavage furrow; and the central spindle, an array of anti-parallel and interdigitating microtubules, which is essential for positioning the cleavage furrow, keeping the dividing genomes apart, and for the final separation, i.e. abscission, of the daughter cells[1]. The contractile ring and the central spindle are composed of several proteins and protein complexes that act as structural and regulatory factors that control the formation, dynamics and stability of these cytoskeletal structures throughout cytokinesis[1,2]. Like in many other processes during cell division, the functions and interactions of these proteins are often regulated by reversible post-translational modifications, including phosphorylation/de-phosphorylation mostly mediated by serine/threonine kinases and their counteracting phosphatases[3]. During furrow ingression, the contractile ring compacts the central spindle and, after completion of furrow ingression, the two daughter cells remain connected by an intercellular bridge, which contains at its center an organelle, the midbody, composed of a multitude of proteins that have diverse functions. Some midbody proteins are former components of the contractile ring and central spindle, while others are specifically recruited during the slow midbody maturation process that ultimately leads to the abscission of the two daughter cells[4,5]. All these proteins are arranged in a very precise and stereotyped spatial pattern along the midbody[6], which can be divided in approximately three major regions: the midbody ring, containing mostly former contractile ring components like Anillin and Citron kinase; the midbody central core marked by central spindle proteins such as the centralspindlin complex; and the midbody arms that flank the midbody core and where the chromosomal passenger complex (CPC) and the kinesin KIF20A accumulate[4]. The proper localization, regulation and interactions of all these proteins are essential for the execution of abscission and for preventing incorrect genome segregation[5]. Furthermore, recent evidence indicates that the midbody is also involved in many other processes besides cell division, including cell fate, pluripotency, apical-basal polarity, tissue organization, and cilium and lumen formation[7,8]. Therefore, the characterization of the intricate midbody protein interaction

networks (i.e., interactome) and their regulation is essential for understanding how this organelle executes its multiple functions.

In this study, we report the first characterization of the midbody interactome identified by affinity purifications coupled with mass spectrometry (AP-MS) of ten key midbody components. This valuable resource provides a molecular "blueprint" of the intricate connections amongst midbody components that will be pivotal in dissecting the multiple functions of this organelle. In support of this, our initial analysis of the midbody interactome already revealed a plethora of novel interactions and highlighted a new role of the PP1β-MYPT1 phosphatase in regulating the dynamics of central spindle microtubules by antagonizing Aurora B phosphorylation of the centralspindlin component MKLP1 in late cytokinesis.

Results

Citron kinase, a key midbody organizer, interacts with many proteins specifically during cytokinesis

Citron kinase (CIT-K) is a contractile ring component that acts as a major midbody organizer by interacting with several midbody components, including the CPC and centralspindlin, and by maintaining their correct localization and orderly arrangement[9,10]. As a first step towards the characterization of the midbody interactome, we used a human HeLa cell line stably expressing CIT-K tagged with GFP[11] to identify the CIT-K interactomes at different cell cycle stages - S phase, metaphase and telophase – by AP-MS (Fig. 1a-b and Supplementary Data S1). We found that the number of CIT-K interactors consistently increased in telophase in three separate replicates, confirming the important role of this kinase in cytokinesis (Fig. 1b). Notably, only 62 proteins, including the bait CIT-K and two of its known partners, the contractile ring component Anillin and the kinesin KIF14[12,13], were common to all three mitotic stages (Fig. 1b and Supplementary Data S1), indicating that our AP-MS methodology identifies specific interactions and generates little noise.

To assess whether CIT-K was required for recruiting some of these interactors to the midbody, we used SILAC-based quantitative MS to characterize and compare the proteomes of midbodies purified from telophase HeLa cells treated with either CIT-K or control siRNAs (Fig. 1c, Supplementary Fig. S1 and Supplementary Data S2). Only minor differences in the levels of a few midbody proteins were identified, including Filamin B, the kinesin KIFC1, Aurora A kinase and its interactor TPX2 (Fig. 1d, Supplementary Table S1 and Supplementary Data S2). Although some of

these differences were significant and validated by Western blot (Fig, 1e and Supplementary Table S1), overall our results did not indicate a major role for CIT-K in recruiting midbody proteins and reinforced the evidence that CIT-K has a very specific function in the organization of this organelle.

Finally, it is important to point out that our midbody proteome contains a significant higher number of proteins than a previous study[14]. This most likely reflects the considerable advancements in MS technology in recent years rather than a difference in the midbody purification protocols.

The midbody interactome is composed of common and specific networks

To further our knowledge of the interaction networks within the midbody, we expanded our AP-MS experiments to include nine additional baits, all proteins that are well known to play key roles in midbody assembly and cytokinesis and display specific and distinct localization patterns (Table 1). AP-MS analysis of the interactions of these ten baits in telophase revealed a complex midbody interactome comprising almost 3000 proteins (Supplementary Data S3 and S4), which included the majority of midbody proteome components and showed a Gene Ontology (GO) enrichment profile very similar to the midbody proteome characterized in our SILAC experiments (Fig. 2 and Supplementary Data S4-S5). The overlap and similarity between the two datasets is highly significant considering that they were obtained using two completely different experimental procedures (see Methods). The midbody interactome contains complex networks shared by several baits as well as networks specific for each bait or for just a few baits (Fig. 3a to d). Interestingly, even proteins strictly related, like the two ESCRT-III paralogs CHMP4B and CHMP4C, showed distinct specific networks (Fig. 3a). Analysis of the interactome networks further confirmed the specificity and selectivity of our AP-MS methodology. For example, the contractile ring component Anillin presents a specific interaction network that include the vast majority of septin proteins (Fig. 3b), which are known to be recruited by Anillin to midbody[15,16]. Similarly, the mitotic kinase Polo-like kinase 1 (Plk1) was only identified with the bait PRC1 (Fig. 3d), which directly binds to and recruits Plk1 to the central spindle and midbody in both human and Drosophila cells[17,18].

Our midbody interactome revealed a plethora of novel interactions that can lead to the discovery of novel structural and regulatory networks present within this organelle. For example, in the network specifically shared by CIT-K and its partner KIF14, we identified the cyclin-dependent kinase 1 (Cdk1) and the microtubule depolymerizing kinesin KIF2C/MCAK (Fig. 3c), both also found in the midbody proteome (Supplementary Data S2 and S4). KIF2C regulates microtubule dynamics

during mitotic spindle assembly[19], but it has not been implicated in cytokinesis. Cdk1, in complex with cyclin B, is well known to promote mitotic entry and to regulate multiple mitotic events until anaphase, when most of the complex is inactivated through degradation of cyclin B. However, a pool of Cdk1/cyclin B has been described to accumulate at the midbody where it appears to promote abscission[20]. Our data not only indicate a potential new role for KIF2C in cytokinesis and confirm the presence and function of Cdk1/cyclin B at the midbody, but also suggest that the association with CIT-K and KIF14 might be important for their localization and/or function.

PP1β-MYPT1 phosphatase regulates central spindle microtubule dynamics in late cytokinesis

Cell division is regulated by post-translational modifications, including phosphorylation mostly mediated by serine/threonine kinases and counteracting phosphatases. Although most kinases involved in cytokinesis are known, the identity and function of their opposing phosphatases is just emerging[4,21]. To address this nescience, we generated a midbody interactome serine/threonine phosphorylation sub-network by extracting from the entire interactome dataset proteins whose full names (Uniprot field:protein names) contained the terms 'kinase' and 'phosphatase' but excluded those containing 'tyrosine' (Fig. 3d). The most frequent and abundant phosphatases belong to the PP1 family (Supplementary Table S2), and the top scores include the three PP1 catalytic subunits - α, β and γ - and the PPP1R12A regulatory subunit, also known as myosin phosphatase target subunit 1, MYPT1. PP1γ was described to accumulate at the cleavage site[22] and we found that all four PP1 phosphatases localized to the midbody ring in late cytokinesis, and PP1β and MYPT1 also accumulated at the cleavage furrow in early telophase (Fig. 4a-d). The signals detected by these antibodies are specific because they were strongly reduced after siRNA treatments in both immuno-fluorescence and Western blot analyses (Fig 4a-e). We then investigated if siRNA-mediated depletion of these phosphatases caused cytokinesis failure. siRNA of *PP1β* and *MYPT1* caused the highest increases in multinucleation (a readout of cytokinesis failure), 4.3 and 8.4 fold, respectively (Fig. 4g-h). PP1α depletion did not result in an increase of multinucleated cells and only a very modest increase (1.6-fold) was observed after PP1γ siRNA(Fig. 4h). However, combined depletion of these two closely related catalytic subunits resulted in a 2.9-fold increase in multinucleated cells (Fig. 4h), suggesting that they could act redundantly and/or synergistically in cytokinesis. In sum, our results indicated that, of all four phosphatases, PP1β and MYPT1 were the two most strongly required for cytokinesis (Fig. 4e, g, and h), which is consistent with the evidence that MYPT1 is a

known PP1β regulatory subunit[23]. MYPT1 was reported to antagonize Plk1 during mitotic spindle assembly and to be required for cytokinesis[24], but its exact role in cytokinesis was not investigated, probably assuming that it was required to de-phosphorylate the myosin regulatory light chain (MRLC) at the contractile ring. We found that, indeed, the levels of both mono(pS19)- and di(pT18 pS19)-phosphorylated MRLC levels were elevated in MYPT1 depleted cells (Fig 5a-b), which had also an abnormal cytoskeleton and numerous cortical blebs (Fig. 4f). However, mitotic exit was not affected after MYPT1 siRNA, as cyclin B levels dropped in anaphase and de-phosphorylation of two phospho-epitopes, PRC1 pT481[25] and tri-phospho CHMP4C[26,27], known to occur upon mitotic exit, was not affected (Fig. 5b). *MYPT1* siRNA cells could successfully complete furrowing, although the central spindle appeared longer and bent upwards in late cytokinesis (Fig. 5a and Supplementary Video S1 to S4). Time-lapse analysis of chromosome and microtubule dynamics during cell division revealed that *MYPT1* siRNA caused abnormal cortical contractility that did not prevent furrow formation and ingression, albeit furrowing was faster than in control cells (Fig. 6a to c, and Supplementary Videos S5 to S8), likely because of hyper-phosphorylated MRLC. Notably, after completion of furrow ingression, *MYPT1* siRNA cells failed to maintain a robust central spindle, which became very thin, bent and long, and sometime snapped (Fig. 6a-h, and Supplementary Video S6). Consistent with these phenotypes, in the majority of *MYPT1* siRNA cells abscission either failed or did not occur during the period of filming (Fig. 6b and Supplementary Video S7). Even when *MYPT1* siRNA cells could successfully separate, abscission was significantly delayed (Fig. 6c). Furthermore, in MYPT1 depleted cells, the midbody was not properly assembled as many of its components were stretched along the central spindle and lost their precise arrangement: Aurora B kinase spread from the midbody arms into the midbody core (Fig. 6d), the kinesin MKLP1 and the microtubule bundling protein PRC1 failed to localize as two juxtaposed discs (Fig. 6e-g and Fig. 7a), and CIT-K assembled into misshapen rings that often collapsed (Fig. 6e and 6h). Electron microscopy analysis showed that *MYPT1* siRNA midbodies contained fewer microtubules and an abnormal midbody matrix compared to control cells (Fig. 6i). These central spindle and midbody defects are not linked to abnormal cortical contractions or adhesion problems because they were also observed in less adherent HeLa S3 cells (Supplementary Fig. S2), which have much less phosphorylated MRLC and do not form cortical blebs after MYPT1 depletion (Supplementary Fig. S2 and data not shown). Furthermore, very similar results were obtained in immortalized, non-transformed RPE-1 cells (Supplementary Fig. S3), indicating a general requirement for MYPT1 in cytokinesis in different cell types. Finally, almost identical phenotypes were observed after *PP1β* siRNA (Fig. 4b and

Supplementary Fig. S4), further supporting that MYPT1 is acting as a regulatory subunit for PP1β in late cytokinesis.

PP1β de-phosphorylates the centralspindlin component MKLP1/KIF23

Central spindle assembly depends on various microtubule associated proteins (MAPs)[2], including two key protein complexes: centralspindlin, a hetero-tetramer composed of two MKLP1 and two RacGAP1 subunits, and the PRC1-KIF4A complex. These MAPs have been shown to interact and cooperate to increase the robustness of the central spindle[28]. To understand the molecular mechanisms underpinning the phenotypes observed after MYPT1-PP1β depletion, we investigated whether centralspindlin could be one of the substrates of this phosphatase. Centralspindlin clustering at the central spindle midzone is necessary for its localization and function and requires phosphorylation of the evolutionarily conserved MKLP1 S708 residue by Aurora B[29]. MYPT1 depletion caused a significant increase in MKLP1 S708 phosphorylation at the midbody (Fig. 7a-b), reduced the association of this kinesin with its RacGAP1 partner and almost completely abolished its interaction with PRC1 and PP1β, but only mildly affected the association with CIT-K (Fig. 7c). MKLP1 contains a highly conserved VQF motif 80 amino acids downstream of S708 (aa 786-788; Fig. 7d and Supplementary Fig. S5a) that partially matches the RVxF consensus binding site for PP1 catalytic subunits[30]. We found that full length MKLP1 and PP1β interacted when co-expressed in yeast (Fig. 7e) and that the MKLP1 C-terminal region (aa 620-858) purified from bacteria was also able to pull down PP1β *in vitro* (Fig. S5b-c), indicating that PP1β directly binds to the MKLP1 C-terminus. $MKLP1_{620-858}$ was dephosphorylated at S708 by PP1β *in vitro* (Fig. 7f-g) and when the VQF residues were mutated to AQA the binding of MKLP1 to PP1β was reduced (Fig. 7e and S5b-c) and $MKLP1_{620-858}$ dephosphorylation by PP1β *in vitro* was less efficient (Fig. 7f-g). To assess the role of MKLP1 de-phosphorylation by PP1β *in vivo*, we generated cell lines stably expressing GFP-tagged versions of either wild type MKLP1 or of the mutant containing the AQA mutation at residues 786-788. Silencing MKLP1 by using an siRNA directed against its 3' UTR that is absent in the GFP-tagged transgenes severely impaired central spindle assembly and cleavage furrow ingression (Fig. 7h, top panels). The very few *MKLP1* siRNA cells that managed to complete furrowing had very thin central spindles and abnormal PRC1 localization (Fig. 7h), resembling *MYPT1* siRNA cells (Fig. 6). The $MKLP1^{AQA}$ mutant rescued cytokinesis failure after depletion of endogenous MKLP1 much less efficiently than the wild type counterpart (Fig. 7h-i). Importantly, $MKLP1^{AQA}$ could successfully

rescue the initial stages of cytokinesis, but in late telophase central spindles appeared thin and PRC1 spread along central spindle microtubules (Fig. 7h, bottom panels), again similar to *MYPT1* siRNA cells (Fig. 6). Together, these results indicate that PP1β dephosphorylates MKLP1 at S708 in late cytokinesis via association with the VQF motif and that this de-phosphorylation is important for MKLP1 function in late cytokinesis.

Discussion

Our characterization of the midbody interactome and proteome represents a significant advance in understanding the complex and intricate protein-protein interactions of this organelle. It is the first interactome derived from experimental data and provides a much more realistic and accurate picture than a previous bioinformatics study[31]. The overlap and highly similar GO enrichment profiles of the interactome and proteome datasets (Fig. 2) strongly support the validity of our approach and methodology. As expected, both datasets are enriched in proteins involved in mitosis and cytokinesis, but they also show a significant enrichment in proteins involved in chromatin assembly and mRNA processing and translation (Fig. 2 and Supplementary Data S4-S5). Although unpredicted, these findings are consistent with the identification of histones at the midbody[32] and the evidence that the RNA-binding protein ATX-2 is involved in post-transcriptional regulation of PAR-5 levels at the midbody[33]. They also highlight the possibility that the midbody may function as a translational hub, which could indicate a mechanism by which asymmetric inheritance of the midbody imparts genetic information in cell fate and carcinogenesis[34,35]. The identification of common and specific networks of midbody proteins could serve to dissect main regulatory mechanisms and pathways for midbody function as well as to identify specific roles for each of the ten baits used in our study. Together, these specific and common interaction networks will undoubtedly provide an extremely valuable resource for understanding the emerging multifaceted biological roles of this organelle. However, our interactome analysis is limited to one cell type and it is possible that different proteins and protein-protein interactions exist in midbodies of different cell types. Nevertheless, our study provides the first molecular 'blueprint' of the interaction networks in the midbody, which can serve to identify major nodes, hubs and pathways that may facilitate the analysis and comparison of midbodies in other cellular and developmental contexts.

The most abundant and frequent phosphatases identified in our midbody interactome are members of the PP1 family (Fig. 3d and Supplementary table S2). This was somehow unexpected as

only PP2A phosphatases had been previously implicated in the regulation of cytokinesis[36,37] and just very recently a role in abscission was described for PP1γ and its targeting co-factor RIF1[38], which was also identified in both our midbody interactome and proteome (Supplementary Data S4). Therefore, our results expand the repertoire of PP1 functions during mitotic exit and indicate that MYPT1-PP1β is required to regulate the pace of cleavage furrow ingression and to form strong and stable central spindles and midbodies in late cytokinesis (Fig. 6a-c). Cytokinesis failure after *MYPT1* siRNA occurs predominantly at a late stage, after completion of furrow ingression (Fig. 6b), highlighting for the first time an unanticipated role of MYPT1 in this phase of cell division. Our results indicate that MYPT1/PP1β regulates the dynamics of the two major cytokinetic structures, the actomyosin contractile ring and the central spindle, by de-phosphorylating different substrates. In line with its established role, our data indicate that MYPT1-PP1β de-phosphorylates MRLC to control the contractility of the actomyosin ring during furrow ingression (Fig. 5), but also unexpectedly reveal that MYPT1-PP1β controls the dynamics of central spindle microtubules in late cytokinesis (Fig. 6). Our results suggest that the latter could be mediated, at least in part, through de-phosphorylation of MKLP1, and most likely of other MAPs, in order to antagonize Aurora B and possibly other mitotic kinases, like Plk1 and CIT-K, in late cytokinesis (Figs. 6 and 7). We surmise that MKLP1 de-phosphorylation by PP1β modulates centralspindlin clustering in order to promote different functions of this complex in late cytokinesis, like its close association with other midbody proteins such as PRC1. This, in combination with de-phosphorylation of additional midbody components, would contribute to MYPT1-PP1β-mediated regulation of central spindle microtubule dynamics and midbody architecture in late cytokinesis. In sum, our findings indicate that temporal changes in the spatial distribution of kinases and counteracting phosphatases during cytokinesis control the phosphorylation status, and consequently the activity, of cytokinesis proteins as illustrated in Fig. 8. In early telophase MYPT1-PP1β localizes to the cortex of the ingressing furrow (see Fig. 4) where it can de-phosphorylate MRLC to antagonize Rho kinase, but has no or little access to the centralspindlin pool that accumulate at the central spindle midzone, which is instead highly phosphorylated by Aurora B and can therefore form clusters. However, after completion of furrow ingression, MYPT1-PP1β accumulates at the midbody ring whereas Aurora B is slowly degraded and accumulates at the midbody arms. This allows de-phosphorylation of MKLP1 at S708, which could strengthen the association of centralspindlin with other midbody proteins, in particular PRC1. This change in the phosphorylation status of MKLP1, and most likely of other midbody components, is

important for maintaining a robust central spindle and for establishing proper midbody architecture.

Finally, our data show that MYPT1 is required for the association of MKLP1 and PP1β in telophase cells (Fig. 7c) and that PP1β requires the VQF sub-optimal binding motif of MKLP1 to select its target S708 residue (Fig. 7). However, our current knowledge of PP1 function indicates that PP1β cannot simultaneously interact with both MYPT1 and MKLP1 through their (R)VxF motifs. One possible explanation could be that MYPT1 is necessary to initially bring PP1β in proximity of MKLP1, but then a pool of PP1β could dissociate from MYPT1 to interact with MKLP1 through its less efficient VQF site to de-phosphorylate S708. Future studies can clarify whether such a two-step mechanism of action does indeed exist and how widely it is employed by PP1 catalytic subunits.

Methods

Molecular Biology. The coding sequence for PP1β was amplified by PCR using the Addgene plasmid 31677 as a template to create an "entry" clone in pDONR221 using Gateway technology (ThermoFisher) as described[39]. The plasmid pEGFP-C1::MKLP1 was previously described[29]. The QuikChange Lightning Site-Directed Mutagenesis Kit (Agilent) was used to generate the PP1β phosphatase "dead" mutant (harbouring the mutations D94N and H124N) and the pEGFP-C1::MKLP1^{AQA} plasmid containing two substitutions in the VQF$_{786-788}$ binding site for PP1β. The sequence of all DNA constructs were verified by sequencing (Source BioScience).

Cell culture and treatments. HeLa Kyoto were maintained in DMEM (Sigma) containing 10% Fetal Bovine Serum (Sigma) and 1% pennicillin/streptomycin (Invitrogen) at 37°C and 5% CO_2. HeLa cell lines stably expressing GFP or Flag-tagged transgenes (listed in Table S2) were cultured in the same medium with the addition of appropriate selection antibiotics (puromycin and/or G418). The HeLa Kyoto cell line stably expressing GFP::tubulin and H2B::mCherry was described[40]. hTERT RPE-1 cells were cultured in DMEM/F12 (Sigma) containing 2mM L-glutamine, 10% Fetal Bovine Serum (Sigma) and 1% pennicillin/streptomycin (Invitrogen) at 37°C and 5% CO_2.

For RNA interference the following siRNAs were used: scrambled sequence control: 5'-AACGTACGCGGAATACTTCGA-3', CIT-K: 5'-ATGGAAGGCACTATTTCTCAA-3', PP1α: 5'-AAGAGACGCTACAACATCAAA-3', PP1β: 5'-ACGAGGAUGUCGUCCAGGAA-3' and 5'-GUUCGAGGCUUAUGUAUCA-3', PP1γ: 5'-ACAUCGACAGCAUUAUCCAA-3' and 5'-

AGAGGCAGUUGGUCACUCU-3', MYPT1: 5'-AGUACUCAACCAUAAUUAA-3', MKLP1 3' UTR: 5'-AAGCAGUCUUCCAGGUCAUCUUU-3', using Lipofectamine RNAiMAX (Invitrogen) following the manufacturer's instructions. All these siRNAs have been previously validated for specificity and efficacy[10,24,29,41].

Cell lines stably expressing MKLP1 or MKLP1^{AQA} constructs were generated by transfecting $2x10^6$ HeLa Kyoto cells with 10 μg of plasmid DNA using the Neon Transfection System (ThermoFisher) using manufacturer's instructions. After 48 hours cells in 100 mm culture dish were selected in complete selective medium containing 400 μg/ml G418 for approximately two weeks until colonies became visible. Individual colonies were picked, cultured under resistance and tested for expression of the construct by Western blot and immunofluorescence. To generate the cell line expressing Aurora B::GFP, HeLa cells (originally from ATCC) were transfected with the mammalian expression vector pcDNA3.1 containing the coding sequence of human Aurora-B, C-terminally fused to GFP, using FuGENE transfection reagent according to the manufacturer's instructions. 24h post-transfection G418 was added to the medium (500 μg/ml), and cells incubated for a further 7 days. The population was then expanded and FACS sorted on the GFP signal, and maintained under G418 selection.

HeLa cells were synchronized in S phase by double thymidine block. Cells were first arrested in S phase by the addition of 2 mM thymidine (Sigma-Aldrich) for 19 h, washed twice with phosphate-buffered saline (PBS) and released for 5 h in fresh complete medium. After release, cells were incubated again for 19 h in complete medium containing 2 mM thymidine, washed twice with PBS, released in fresh medium for 10 minutes, harvested by centrifugation at 1000 *g* for 3 minutes, washed in PBS, frozen immediately in dry ice and stored at -80°C. To synchronize HeLa Kyoto in metaphase and telophase, we used a thymidine-nocodazole block and release procedure. Cells were first arrested in S phase by a single thymidine treatment as described above, washed twice with phosphate-buffered saline (PBS) and released for 5 h in fresh complete medium. Cells were then cultured for additional 13 h in fresh complete medium containing 50 ng/ml nocodazole (Sigma-Aldrich) and then harvested by mitotic shake-off. Mitotic cells were washed three times with PBS, and either released for 30 min in fresh medium containing 10 μM MG132 (Sigma) to collect cell in metaphase or released in just fresh medium for 90 min to collect cells in telophase. Cells were then harvested by centrifugation and frozen in dry ice.

Midbody purification. For SILAC experiments, HeLa S3 cells were grown in DMEM lacking Arg and Lys (Invitrogen), and supplemented with 10% (v/v) 1 kDa dialyzed FBS (Sigma-Aldrich), 1% (v/v) penicillin/streptomycin and either unlabelled Arg and Lys or L-[$^{13}C_6$,$^{15}N_4$] Arg and L-[$^{13}C_6$,$^{15}N_2$] Lys (Cambridge Isotope Laboratories) at concentrations of 42 μg/ml (Arg) and 72 μg/ml (Lys). Trypsin-EDTA was used to split cells as usual. However, as this solution might contain some non-isotopically labelled amino acids, detached cells were pelleted at 250 *g* for 3 min and washed once with sterile phosphate-buffered saline (PBS) before being re-seeded in fresh medium.

To purify midbodies, $2.8x10^7$ HeLa S3 cells were plated into three three-layer tissue culture flasks, 525 cm^2 (BD Biosciences), for a total of $8.4x10^7$ cells per condition. Cells were synchronized using the thymidine-nocodazole block and release procedure described in the previous section. After nocodazole washout cells were incubated for 2 h in fresh medium containing 10 μM MG132 (Sigma-Aldrich) to further increase the effectiveness of the synchronization, and then incubated at 37ºC for 80 min after release from MG132. Just before collection, 5 μg/ml taxol (Sigma-Aldrich) was added to the medium for 2-3 min to stabilize microtubules in vivo. Cells were then transferred into a 50 ml conical tube and collected by centrifugation at 250 *g* for 3 min. After one wash with pre-warmed H_2O, cells were gently resuspended in 25 ml of swelling solution (1 mM PIPES pH 7.0, 1 mM $MgCl_2$, 5 μg/ml taxol and Roche Complete Protease Inhibitors) and immediately centrifuged at 250 *g* for 3 min. The cell pellet was then resuspended in 40 ml of lysis buffer (1 mM PIPES pH 7, 1 mM EGTA, 1 % [v/v] NP-40, 5 μg/ml taxol, 3 U/ml DNAse I, 10 μg/ml RNAse A, 1 U/ml micrococcal nuclease, and Roche Complete Protease Inhibitors) and vortexed vigorously for 1 min. After the addition of 0.3 volumes of cold 50 mM 2-(N-mopholino)ethanesulfonic acid (MES) pH 6.3, the sample was incubated on ice for 20 min and then centrifuged at 200 *g* for 10 min at 4°C. The supernatant was transferred to a new tube and centrifuged at 650 *g* for 20 min at 4°C to pellet midbodies. The midbody pellet was then resuspended in 4 ml of 50 mM MES pH 6.3 and centrifuged through a 25 ml glycerol cushion (40% [w/v] glycerol diluted in 50 mM MES pH 6.3) at 2,800 *g* for 45 min at 4°C. After removal of the glycerol cushion, the midbody pellet was washed with 2 ml of 50 mM MES pH 6.3, transferred to a 15 ml conical tube and centrifuged at 2,800 *g* for 20 min at 4ºC. For mass spectrometry (MS) analyses, after removing as much liquid as possible, the midbody pellet was resuspended in 100 μl of 50 mM MES pH 6.3 and 900 μl of cold acetone were added to the tube, which was then vortexed and incubated for 10-15 min at -20°C. The sample was then centrifuged at 3,500 *g* for 10 min at 4°C, the supernatant was carefully discarded and the pellet was

left to dry for 5-10 min at room temperature (RT). Precipitated proteins were stored at -80°C until further processing.

Affinity purification (AP). For large-scale AP of GFP-tagged proteins and associated partners, cells were plated at 1/6 confluence in either six 175 cm^2 flasks or in two three-layer 525 cm^2 tissue culture flasks (BD Biosciences) and after 24 hours synchronized at different stages of the cell cycle as described in the previous section. APs were then carried out essentially as described[42]. Briefly, the cell pellet was resuspended in 5 ml of lysis buffer (20 mM Tris-HCl, 150 mM NaCl, 2 mM $MgCl_2$, 1 mM EGTA, 0.1% [v/v] NP-40, 1 mM DTT, 5% [v/v] glycerol and Roche Complete Protease Inhibitors) and homogenized using a high-performance disperser (Fisher). The homogenate was clarified by centrifugation at 750 *g* for 15 min at 4°C and the supernatant was incubated with 200 µl of GFP-Trap_MA magnetic beads (ChromoTek) for 4 h on a rotating wheel at 4°C. Beads were then washed four times using a magnetic stand in 10 ml of lysis buffer for 5 min on a rotating wheel at 4°C, transferred to a new tube and washed one more time in 10 ml of PBS. After removing as much liquid as possible, beads were stored at -80°C before being analyzed by liquid chromatography coupled with tandem MS (LC-MS/MS; see section below). Most of the AP experiments were carried out in duplicates, with the exception of CIT-K::AcGFP, which was in triplicate for each cell cycle phase, and GFP::PRC1, which was performed only once.

Mass spectrometry (MS) analyses. For the analysis of AP samples, beads were digested with trypsin and processed as previously described[10]. To analyze SILAC midbody samples, proteins were resuspended in lysis buffer (100 mM Tris pH 8.5, 100 mM tris[2-carboxyethyl]phosphine, 4%SDS [w/v], 8 M urea) and alkylated by the addition of iodoacetamide at a final concentration of 40 mM for 30 min at room temperature in the dark. Samples were then mixed with NuPAGE LDS 4x Sample Buffer (Invitrogen), boiled for 5 min at 90°C and loaded on NuPAGE Novex 4–12% Bis-Tris Protein Gels (Invitrogen). Gels were then fixed for 30 min at RT in fixing solution (40% [v/v] methanol, 2% [v/v] acetic acid) and stained overnight with Brilliant Blue G-Colloidal Concentrate (Sigma-Aldrich), according to the manufacturer's instructions. Each gel lane was then excised into ~10 bands. Gel bands were cut into smaller pieces, de-stained completely in 50 mM ammonium bicarbonate/50% (v/v) acetonitrile at 37°C, and dehydrated in pure acetonitrile for 15 min. Gel pieces were then rehydrated in 50 mM ammonium bicarbonate and digested with Trypsin (Sequencing Grade, Roche) overnight at 37°C. Peptides were extracted from gel pieces twice for 30 min at 37°C in 50% (v/v)

acetonitrile/0.5% (v/v) formic acid, dried in a SpeedVac (Thermo Scientific), and resuspended in 0.5% (v/v) formic acid. For LC-MS/MS analysis of SILAC samples, an LTQ Orbitrap Velos mass spectrometer (Thermo Scientific) coupled with an Ultimate 3000 Rapid Separation LC nano ultra high pressure HPLC system (Dionex) was used. Peptides were loaded and desalted on a PepMap C18 precolumn (5µ-beads, 100 µm x 20mm, Dionex) and then separated on a PepMap analytical column (2 µm beads, 75 µm x 50 cm, Dionex) over a 60 min linear gradient (90 min/cycle) of 4–34% (v/v) acetonitrile/0.1% (v/v) formic acid at a flow rate of 0.3 µl/min. The LTQ Orbitrap Velos mass spectrometer was operated in the "top 10" data-dependent acquisition mode where the preview mode was disabled. The Orbitrap full scan was set at m/z 380–1600 with a resolution of 60,000 at m/z 400. The 10 most abundant multiply charged precursor ions, with a minimal signal above 2000 counts, were dynamically selected for collision-induced dissociation fragmentation (MS/MS) in the LTQ Velos ion trap, and the dynamic exclusion was set ±20 ppm within 45 sec. The AGC and maximum injection time for Orbitrap were set at 1e6 and 200 msec, and 1e4 and 150 msec for ion trap.

MS data analysis. For protein identification in the SILAC experiments, the raw files were processed using MaxQuant (version 1.4.0.8) and the Andromeda search engine[43-45]. In all cases, peptides were searched against the UniProt human database concatenated with reversed copies of all sequences and supplemented with frequently observed contaminants. The following search parameters were used: full trypsin specificity was required, a maximum of two missed cleavages were allowed, carbamidomethyl (Cys) was set as a fixed modification, whereas acetylation (Protein N-term), oxidation (Met), deamidation (Asn/Gln) and carbamylation (Lys and N-terminus of protein) were considered as variable modifications. Maximum protein and peptide false discovery rates (FDRs) were set to 1% and minimum required peptide length was set to seven amino acids. Quantification of proteins in the SILAC experiment was performed using MaxQuant[43]. SILAC multiplicity were set to doublets where Lys0/Arg0 and Lys8/Arg10 were selected as light and heavy labels, respectively. Peptides considered for quantification were unique and razor peptides including unmodified, and modified with carbamidomethylated (Cys), acetylated (Protein N-term), oxidated (Met), carbamylated (Lys and N-term) and deamidated (Asn/Gln). The re-quantification feature was enabled. Statistical evaluation of MS results generated by MaxQuant was performed using Perseus[43].

For the identification of proteins from AP experiments, raw MS/MS data were analyzed using the MASCOT search engine (Matrix Science). Peptides were searched against the UniProt human sequence database and the following search parameters were employed: enzyme specificity was set to trypsin, a maximum of two missed cleavages were allowed, carbamidomethylation (Cys) was set as a fixed modification, whereas oxidation (Met), phosphorylation (Ser, Thr and Tyr) and ubiquitylation (Lys) were considered as variable modifications. Peptide and MS/MS tolerances were set to 25 parts per million (ppm) and 0.8 daltons (Da). Peptides with MASCOT Score exceeding the threshold value corresponding to <5% False Positive Rate, calculated by MASCOT procedure, and with the MASCOT score above 30 were considered to be positive.

Computational and statistical analyses. We used in-house written Perl scripts to combine the Mascot data from the replicates of AP-MS experiments for each bait and to compare them with datasets obtained from AP-MS experiments using HeLa cells expressing GFP alone at the same cell cycle stage (S phase, metaphase or telophase) in order to eliminate non-specific hits. Prey hits absent from these GFP negative controls were classed as being specific. Additional common contaminants, such as keratins and haemoglobin, were eliminated manually. The filtered data (Supplementary Data S3) were then analyzed and visualized using Cytoscape (version 3.7.0).

To generate the serine/threonine phosphorylation sub-network, we searched the interactome dataset for proteins whose Uniprot "protein names" field contained the terms 'kinase' and 'phosphatase' but not 'tyrosine' via grep in the Unix command line. This generated a dataset of 190 proteins that was subsequently manually curated to eliminate proteins that were not directly involved in phosphorylation/de-phosphorylation, such as kinase-associated proteins for example. The final list of 136 proteins was entered into a raw tab-delimited text file and then imported into Cytoscape to generate the network shown in Fig 3d.

GO enrichment analysis was performed using PANTHER[46]. Prism8 (GraphPad) and Excel (Microsoft) were used for statistical analyses and to prepare graphs.

Time-lapse imaging. For time-lapse experiments, HeLa Kyoto cells expressing GFP:tubulin and H2B::mCherry were plated on an open μ-Slide with 8 wells (Ibidi, 80826) 30 hours after RNAi treatment. Imaging was performed on a Leica DMi8 CS AFC Motorised Research Inverted Digital Microscope. Images were collected with a 40x/1.30 NA HC Plan APO CS2 - OIL DIC 240 μm objective and excitation Lasers of Argon (65mW, 488nm) and of DPSS (20mW, 561nm). We used the

Application Suite X software (LAS-X; Leica) for multidimensional image acquisition. Specimens were maintained at 37°C and 5% CO_2 via a chamber, and z-series of fourteen, 1-µm sections were captured at 2 min intervals. All images were processed using Fiji[47] to generate maximum intensity projections, to adjust for brightness and contrast, and to create the final movies.

Fluorescence microscopy. HeLa cells were grown on microscope glass coverslips (Menzel-Gläser) and fixed in either PHEM buffer (60 mM Pipes, 25 mM Hepes pH 7, 10 mM EGTA, 4 mM $MgCl_2$, 3.7% [v/v] formaldheyde) for 12 min at room temperature or in ice-cold methanol for 10 min at -20°C. They were then washed three times for 10 min with PBS and incubated in blocking buffer (PBS, 0.5% [v/v] Triton X-100 and 5% [w/v] BSA) for 1 h at room temperature. Coverslips were incubated overnight at 4°C with the primary antibodies indicated in the figure legends, diluted in PBT (PBS, 0.1% [v/v] Triton X-100 and 1% [w/v] BSA). The day after, coverslips were washed twice for 5 min in PBT, incubated with secondary antibodies diluted in PBT for 2 h at RT and then washed twice with PBT and once with PBS. Coverslips were mounted on SuperFrost Microscope Slides (VWR) using VECTASHIELD Mounting Medium containing DAPI (Vector Laboratories). Phenotypes were blindly scored by at least two people independently. Images were acquired using a Zeiss Axiovert epifluorescence microscope equipped with MetaMorph software. Fiji[47] was used to generate maximum intensity projections, which were adjusted for contrast and brightness and assembled using Photoshop. Fluorescence intensity values in Fig. 7B were calculated essentially as described[10]. Briefly, mean fluorescence intensity was measured from identically sized areas at the midbody (I_M), in the nucleus (I_N), and in the background (I_B) using Fiji[47] and then normalized values were calculated using the following formula: $[(I_M-I_B) - (I_N-I_B)]/(I_N-I_B) = (I_M-I_N)/(I_N-I_B)$.

Antibodies. The following antibodies were used in this study: mouse monoclonal anti α-tubulin (clone DM1A, Sigma, T9026), rabbit polyclonal anti-β-tubulin (Abcam, ab6046),), mouse monoclonal anti-cyclin B1 (clone GNS1, Santa Cruz, sc-245), mouse monoclonal anti-PP1α (clone G-4, Santa Cruz, sc-271762), mouse monoclonal anti-PP1β (clone A-6, Santa Cruz, sc-365678), mouse monoclonal anti-PP1γ (clone A-4, Santa Cruz, sc-515943), mouse monoclonal anti-CIT-K (BD Transduction Laboratories, 611377), mouse monoclonal anti-MYPT1 (clone C-6, Santa Cruz, sc-514261), (Abcam, ab2254), rabbit polyclonal anti-MKLP1 (clone N19, Santa Cruz Biotechnology, sc-867), rabbit polyclonal anti-phospho MKLP1 pS708[29], rabbit polyclonal anti-tri-phospho CHMP4C pS210 pS214 pS215[27], mouse monoclonal anti-Aurora B (clone AIM-1, BD Transduction

Laboratories, 611082), mouse monoclonal anti-PRC1 (clone C-1, Santa Cruz, sc-376983), rabbit monoclonal anti-phospho PRC1 pT481 (Abcam, ab62366), rabbit polyclonal anti-phospho-histone H3 pS10 (Merck, 06-570), rabbit polyclonal anti-mono-phospho MRLC pS19 (Cell Signaling Technology, 3671), rabbit polyclonal anti-di-phospho MRLC pT18 pS19 (Cell Signaling Technology, 3674), goat polyclonal anti-RacGAP1 (Abcam, ab2270), mouse monoclonal anti-GST (Abcam, ab92), mouse monoclonal anti-MBP (NEB, E8032). Peroxidase and Alexa-fluor conjugated secondary antibodies were purchased from Jackson Laboratories and ThermoFisher, respectively.

Transmission electron microscopy. For electron microscopy analyses, HeLa Kyoto cells were plated on microscope glass coverslips (Menzel-Gläser). Cells were fixed overnight at 4°C in 2.5% [v/v] glutaraldehyde in PBS, post fixed for 1 h in 1% [v/v] OsO_4 in PBS, dehydrated in a graded series of alcohols, embedded in Epon-Araldite resin, and polymerized for 2 days at 60°C. Glass slides were separated from the resin after a short immersion in liquid nitrogen. Sections were obtained with a LKB ultratome, stained with uranyl acetate and lead citrate, and observed and photographed with a FEI Tecnai G2 Spirit transmission electron microscope operating at an accelerating voltage of 100 kV and equipped with a Morada CCD camera (Olympus).

Time course analysis of protein expression and GFP pull down assay. $1.4x10^6$ HeLa Kyoto cells were plated in large - 175 cm^2 - flasks and transfect with siRNAs (800 pmol) directed against either a scrambled sequence (control) or MYPT1. After 24 h, cells were synchronized by thymidine/nocodazole block, released in fresh medium and divided into four 75 cm^2 flasks, and collected after 0, 45, 90 and 120 min as indicated in Fig 7. Proteins were then extracted, separated on a SDS PAGE gel, transferred onto PVDF membrane, and probed to detect the antigens indicated in Fig. 7.

For GFP pull down assay, GFP::MKLP1 HeLa cells were transfected with siRNAs and synchronized in late telophase (120 min after nocodazole release) as described above. Cells were then collected, washed in PBS, frozen in dry ice and stored at -80°C. Cell pellets were resuspended in 0.5 ml of lysis buffer (20 mM Tris-HCl, 150 mM NaCl, 2 mM $MgCl_2$, 1 mM EGTA, 0.1% [v/v] NP-40, 1 mM DTT, 5% [v/v] glycerol, Roche Complete Protease Inhibitors and PhosSTOP Protein Phosphatase Inhibitors) and homogenized using a high-performance disperser (Fisher). The homogenate was clarified by centrifugation at 750 *g* for 15 min at 4°C and the supernatant was incubated with 40 µl of GFP-Trap MA magnetic Beads (ChromoTek) for 4 h on a rotating wheel at

4°C. Beads were then washed four times in 1 ml of lysis buffer for 5 min on a rotating wheel at 4°C, transferred to a new tube and washed one more time in 1 ml of PBS. After removing as much liquid as possible, beads were resuspended in 2x Laemmli sample buffer (Sigma Aldrich), boiled for 5 min and stored at -20°C. Proteins were separated by SDS PAGE, transferred onto PVDF membrane, and probed to detect the antigens indicated in Fig. 7c.

MKLP1 and PP1β binding assay and protein purification in yeast. Interaction between MBP-MKLP1 and GST-PP1β was explored in *S. cerevisiae* using a modification of the method described[48]. Briefly, MBP-MKLP1 proteins (wild type and AQA mutant) were expressed using a derivative of plasmid pMH919 carrying MBP instead of 6His and GST-PP1β using pMH925. Wild type and mutant alleles were amplified by PCR with oligos containing at their 5' 40 bps homologous to pMH919 and pMH925, respectively. All expressing plasmids were obtained by recombination (GAP repair)[49] using strains MGY140 for the MKLP1 constructs and MGY139 [Mat a, ade5, ura3-5, trp1-289, his3, leu2, lys2Δ0, mob1::kanMX4, cdc28::LEU2, pep4::LYS2/YCplac33-MOB1-CDC28] for the PP1β construct. After recombination, strains were crossed and passed on FOA plates to obtain diploid strains stably expressing pairs of MKLP1 and PP1β proteins (see below). For expression and purification, strains were cultivated for 6 h in YPGal to induce the expression of the recombinant proteins. Cell pellets were re-suspended in Breaking Buffer (50 mM Tris-HCl pH 7.5, 250 mM NaCl, 10% glycerol, 0.2% [v/v] NP-40, 5 mM EDTA, 5 mM DTT, Protease Inhibitor cocktail and 1 mM PMFS) and crude extract was obtained by vortexing in presence of glass beads (0.5 mm diameter). MBP-MKLP1 proteins were purified on amylose resin (New England Biolabs), washed 5 times with Washing Buffer (50 mM Tris-HCl pH 7.5, 250 mM NaCl, 0.2% [v/v] NP-40, 5 mM DTT) and eluted with 20 mM maltose. The presence of GST-PP1β bound to MKLP1 was revealed by western blotting using an anti-GST antibody.

PP1β and PP1β^{dead} proteins were expressed and purified as MBP-fusion proteins in *S. cerevisiae* essentially as described above. Briefly, MBP-PP1β proteins were expressed using a derivative of plasmid pMH919 carrying MBP instead of 6His. PP1β and PP1β^{dead} coding sequences were amplified by PCR with oligonucleotides containing at their 5' 40 bps homologous to pMH919. Expressing plasmids were obtained by recombination using strain MGY70 (see below). For expression and purification, strains were cultivated for 6 h in YPGal to induce the expression of the recombinant proteins. Cell pellets were resuspended in Breaking Buffer and crude extract was obtained by

vortexing in presence of glass beads (0.5 mm diameter). MBP-PP1β proteins were purified on amylose resin and eluted with 20 mM maltose as described above.

S. cerevisiae Strain	Pair of expressed proteins
MGY930	MBP/GST-PP1β
MGY931	MBP-MKLP1 and GST
MGY932	MBP-MKLP1 and GST-PP1β
MGY951	MBP-MKLP1^{AQA} and GST-PP1β
MGY960	MBP-PP1β
MGY961	MBP-PP1β^{dead}

***In vitro* GST pull down and phosphatase assays.** DNA fragments coding for MKLP1$_{620-858}$ (wild type and AQA mutant) were generated by PCR and cloned into pDEST15 (Thermo Fisher) to express N-terminal GST tagged polypeptides in *E. coli*. GST-tagged products were then purified using Glutathione Sepharose 4B according to manufacturer's instruction (GE Healthcare).

GST pull downs were carried out essentially as described[50]. Briefly, MBP::PP1β purified from yeast and eluted from beads (see previous section) was mixed with 25 µl of Glutathione Sepharose beads containing purified GST or GST::MKLP1$_{620-858}$ proteins (wild type and AQA mutant). Samples were incubated in 300 µl of NET-N+ buffer (50mM Tris-HCl, pH 7.4, 150mM NaCl, 5mM EDTA, 0.2% NP-40, and a cocktail of Roche Complete Protease Inhibitors) for 60 minutes at 4°C on a rotating wheel and then washed 5 times with 500 µl of wash buffer (50mM Tris-HCl, pH 7.4, 250mM NaCl, 5mM EDTA, 0.2% NP-40, and a cocktail of Roche Complete Protease Inhibitors) followed by centrifugation at 500 *g* for 1 minute. Beads were resuspended in 25 µl of Laemmli SDS-PAGE sample buffer and typically 1/5 was loaded on a 4-20% Tris-Glycine gel for Western blot analysis.

For the phosphatase assay, 10 µg of purified GST-MKLP1$_{620-858}$ proteins (wild type and AQA mutant) bound to beads were phosphorylated *in vitro* with 2 µg of recombinant His-tagged Aurora B (Thermo Fisher) as described[10,27] and then washed three times with 500 µl of phosphatase buffer (50 mM Tris-HCl pH 7.5, 100 mM NaCl, 1mM $MnCl_2$) to remove Aurora B. Beads were then resuspended in 100 µl of phosphatase buffer, divided in 10 aliquots, and each aliquot was incubated with 200 ng of either MBP-PP1β or MBP-PP1β^{dead} enzymes purified from yeast (see previous section) at 30°C with gentle agitation. Samples were collected at 10, 20, 40 and 60 minutes and reactions were immediately stopped with the addition of 2x Laemmli buffer. Proteins were separated by SDS PAGE and analyzed by Western blot with anti-phospho MKLP1 pS708 and anti-GST antibodies.

Chemiluminescent signals were acquired below saturation levels using a G:BOX Chemi XRQ (Syngene) and quantified using Fiji[47].

Data availability

All data are available in the main text or the supplementary materials. The SILAC mass spectrometry proteomics data have been deposited to the ProteomeXchange Consortium via the PRIDE partner repository with the dataset identifier PXD012374. All materials and reagents are available upon request.

References

1 D'Avino, P. P., Giansanti, M. G. & Petronczki, M. Cytokinesis in animal cells. *Cold Spring Harbor perspectives in biology* **7**, a015834, doi:10.1101/cshperspect.a015834 (2015).

2 Douglas, M. E. & Mishima, M. Still entangled: assembly of the central spindle by multiple microtubule modulators. *Semin Cell Dev Biol* **21**, 899-908, doi:S1084-9521(10)00141-2 [pii] 10.1016/j.semcdb.2010.08.005 (2010).

3 Nasa, I. & Kettenbach, A. N. Coordination of Protein Kinase and Phosphoprotein Phosphatase Activities in Mitosis. *Front Cell Dev Biol* **6**, 30, doi:10.3389/fcell.2018.00030 (2018).

4 D'Avino, P. P. & Capalbo, L. Regulation of midbody formation and function by mitotic kinases. *Semin Cell Dev Biol* **53**, 57-63, doi:10.1016/j.semcdb.2016.01.018 (2016).

5 Mierzwa, B. & Gerlich, D. W. Cytokinetic abscission: molecular mechanisms and temporal control. *Dev Cell* **31**, 525-538, doi:10.1016/j.devcel.2014.11.006 (2014).

6 Hu, C. K., Coughlin, M. & Mitchison, T. J. Midbody assembly and its regulation during cytokinesis. *Mol Biol Cell* **23**, 1024-1034, doi:10.1091/mbc.E11-08-0721 (2012).

7 Dionne, L. K., Wang, X. J. & Prekeris, R. Midbody: from cellular junk to regulator of cell polarity and cell fate. *Curr Opin Cell Biol* **35**, 51-58, doi:10.1016/j.ceb.2015.04.010 (2015).

8 Pohl, C. The Midbody and its Remnant in Cell Polarization and Asymmetric Cell Division. *Results Probl Cell Differ* **61**, 165-182, doi:10.1007/978-3-319-53150-2_7 (2017).

9 Bassi, Z. I., Audusseau, M., Riparbelli, M. G., Callaini, G. & D'Avino, P. P. Citron kinase controls a molecular network required for midbody formation in cytokinesis. *Proc Natl Acad Sci U S A* **110**, 9782-9787, doi:10.1073/pnas.1301328110 (2013).

10 McKenzie, C. *et al.* Cross-regulation between Aurora B and Citron kinase controls midbody architecture in cytokinesis. *Open Biol* **6**, 160019, doi:10.1098/rsob.160019 (2016).

11 McKenzie, C. & D'Avino, P. P. Investigating cytokinesis failure as a strategy in cancer therapy. *Oncotarget* **7**, 87323-87341, doi:10.18632/oncotarget.13556 (2016).

12 Gai, M. *et al.* Citron kinase controls abscission through RhoA and anillin. *Mol Biol Cell* **22**, 3768-3778, doi:mbc.E10-12-0952 [pii] 10.1091/mbc.E10-12-0952 (2011).

13 Gruneberg, U. *et al.* KIF14 and citron kinase act together to promote efficient cytokinesis. *J Cell Biol* **172**, 363-372 (2006).

14 Skop, A. R., Liu, H., Yates, J., 3rd, Meyer, B. J. & Heald, R. Dissection of the mammalian midbody proteome reveals conserved cytokinesis mechanisms. *Science* **305**, 61-66, doi:10.1126/science.1097931 (2004).

15 Field, C. M., Coughlin, M., Doberstein, S., Marty, T. & Sullivan, W. Characterization of anillin mutants reveals essential roles in septin localization and plasma membrane integrity. *Development* **132**, 2849-2860 (2005).
16 Renshaw, M. J., Liu, J., Lavoie, B. D. & Wilde, A. Anillin-dependent organization of septin filaments promotes intercellular bridge elongation and Chmp4B targeting to the abscission site. *Open Biol* **4**, 130190, doi:10.1098/rsob.130190 (2014).
17 D'Avino, P. P. *et al.* Recruitment of Polo kinase to the spindle midzone during cytokinesis requires the Feo/Klp3A complex. *PLoS ONE* **2**, e572, doi:10.1371/journal.pone.0000572 (2007).
18 Neef, R. *et al.* Choice of Plk1 docking partners during mitosis and cytokinesis is controlled by the activation state of Cdk1. *Nat Cell Biol* **9**, 436-444, doi:ncb1557 [pii] 10.1038/ncb1557 (2007).
19 Sanhaji, M., Friel, C. T., Wordeman, L., Louwen, F. & Yuan, J. Mitotic centromere-associated kinesin (MCAK): a potential cancer drug target. *Oncotarget* **2**, 935-947, doi:10.18632/oncotarget.416 (2011).
20 Mathieu, J. *et al.* Aurora B and cyclin B have opposite effects on the timing of cytokinesis abscission in Drosophila germ cells and in vertebrate somatic cells. *Dev Cell* **26**, 250-265, doi:10.1016/j.devcel.2013.07.005 (2013).
21 Wurzenberger, C. & Gerlich, D. W. Phosphatases: providing safe passage through mitotic exit. *Nat Rev Mol Cell Biol* **12**, 469-482, doi:10.1038/nrm3149 (2011).
22 Trinkle-Mulcahy, L. *et al.* Time-lapse imaging reveals dynamic relocalization of PP1gamma throughout the mammalian cell cycle. *Mol Biol Cell* **14**, 107-117, doi:10.1091/mbc.e02-07-0376 (2003).
23 Kiss, A., Erdodi, F. & Lontay, B. Myosin phosphatase: Unexpected functions of a long-known enzyme. *Biochim Biophys Acta Mol Cell Res* **1866**, 2-15, doi:10.1016/j.bbamcr.2018.07.023 (2019).
24 Yamashiro, S. *et al.* Myosin phosphatase-targeting subunit 1 regulates mitosis by antagonizing polo-like kinase 1. *Dev Cell* **14**, 787-797, doi:10.1016/j.devcel.2008.02.013 (2008).
25 Jiang, W. *et al.* PRC1: a human mitotic spindle-associated CDK substrate protein required for cytokinesis. *Mol Cell* **2**, 877-885 (1998).
26 Capalbo, L. *et al.* Coordinated regulation of the ESCRT-III component CHMP4C by the chromosomal passenger complex and centralspindlin during cytokinesis. *Open Biol* **6**, doi:10.1098/rsob.160248 (2016).
27 Capalbo, L. *et al.* The chromosomal passenger complex controls the function of endosomal sorting complex required for transport-III Snf7 proteins during cytokinesis. *Open Biol* **2**, 120070, doi:10.1098/rsob.120070 rsob120070 [pii] (2012).
28 Lee, K. Y., Esmaeili, B., Zealley, B. & Mishima, M. Direct interaction between centralspindlin and PRC1 reinforces mechanical resilience of the central spindle. *Nature communications* **6**, 7290, doi:10.1038/ncomms8290 (2015).
29 Douglas, M. E., Davies, T., Joseph, N. & Mishima, M. Aurora B and 14-3-3 coordinately regulate clustering of centralspindlin during cytokinesis. *Curr Biol* **20**, 927-933, doi:10.1016/j.cub.2010.03.055 (2010).
30 Heroes, E. *et al.* The PP1 binding code: a molecular-lego strategy that governs specificity. *FEBS J* **280**, 584-595, doi:10.1111/j.1742-4658.2012.08547.x (2013).
31 Chen, T. C. *et al.* From midbody protein-protein interaction network construction to novel regulators in cytokinesis. *J Proteome Res* **8**, 4943-4953, doi:10.1021/pr900325f (2009).

32 Rinaldo, C. *et al.* HIPK2 controls cytokinesis and prevents tetraploidization by phosphorylating histone H2B at the midbody. *Mol Cell* **47**, 87-98, doi:10.1016/j.molcel.2012.04.029 (2012).
33 Gnazzo, M. M. *et al.* The RNA-binding protein ATX-2 regulates cytokinesis through PAR-5 and ZEN-4. *Mol Biol Cell* **27**, 3052-3064, doi:10.1091/mbc.E16-04-0219 (2016).
34 Ettinger, A. W. *et al.* Proliferating versus differentiating stem and cancer cells exhibit distinct midbody-release behaviour. *Nature communications* **2**, 503, doi:10.1038/ncomms1511 (2011).
35 Kuo, T. C. *et al.* Midbody accumulation through evasion of autophagy contributes to cellular reprogramming and tumorigenicity. *Nat Cell Biol* **13**, 1214-1223, doi:10.1038/ncb2332 (2011).
36 Bastos, R. N., Cundell, M. J. & Barr, F. A. KIF4A and PP2A-B56 form a spatially restricted feedback loop opposing Aurora B at the anaphase central spindle. *J Cell Biol* **207**, 683-693, doi:10.1083/jcb.201409129 (2014).
37 Cundell, M. J. *et al.* The BEG (PP2A-B55/ENSA/Greatwall) pathway ensures cytokinesis follows chromosome separation. *Mol Cell* **52**, 393-405, doi:10.1016/j.molcel.2013.09.005 (2013).
38 Bhowmick, R. *et al.* The RIF1-PP1 Axis Controls Abscission Timing in Human Cells. *Curr Biol* **29**, 1232-1242 e1235, doi:10.1016/j.cub.2019.02.037 (2019).
39 D'Avino, P. P., Savoian, M. S., Capalbo, L. & Glover, D. M. RacGAP50C is sufficient to signal cleavage furrow formation during cytokinesis. *J Cell Sci* **119**, 4402-4408 (2006).
40 Neumann, B. *et al.* Phenotypic profiling of the human genome by time-lapse microscopy reveals cell division genes. *Nature* **464**, 721-727, doi:nature08869 [pii] 10.1038/nature08869 (2010).
41 Lehmann, A., Kliewer, A., Martens, J. C., Nagel, F. & Schulz, S. Carboxyl-terminal receptor domains control the differential dephosphorylation of somatostatin receptors by protein phosphatase 1 isoforms. *PLoS One* **9**, e91526, doi:10.1371/journal.pone.0091526 (2014).
42 Lipinszki, Z. *et al.* Affinity purification of protein complexes from Drosophila embryos in cell cycle studies. *Methods Mol Biol* **1170**, 571-588, doi:10.1007/978-1-4939-0888-2_33 (2014).
43 Cox, J. & Mann, M. MaxQuant enables high peptide identification rates, individualized p.p.b.-range mass accuracies and proteome-wide protein quantification. *Nat Biotechnol* **26**, 1367-1372, doi:10.1038/nbt.1511 (2008).
44 Cox, J. *et al.* A practical guide to the MaxQuant computational platform for SILAC-based quantitative proteomics. *Nat Protoc* **4**, 698-705, doi:10.1038/nprot.2009.36 (2009).
45 Cox, J. *et al.* Andromeda: a peptide search engine integrated into the MaxQuant environment. *J Proteome Res* **10**, 1794-1805, doi:10.1021/pr101065j (2011).
46 Mi, H. *et al.* PANTHER version 11: expanded annotation data from Gene Ontology and Reactome pathways, and data analysis tool enhancements. *Nucleic Acids Res* **45**, D183-D189, doi:10.1093/nar/gkw1138 (2017).
47 Schindelin, J. *et al.* Fiji: an open-source platform for biological-image analysis. *Nat Methods* **9**, 676-682, doi:10.1038/nmeth.2019 (2012).
48 Geymonat, M., Spanos, A. & Sedgwick, S. Production of mitotic regulators using an autoselection system for protein expression in budding yeast. *Methods Mol Biol* **545**, 63-80, doi:10.1007/978-1-60327-993-2_4 (2009).
49 Orr-Weaver, T. L., Szostak, J. W. & Rothstein, R. J. Genetic applications of yeast transformation with linear and gapped plasmids. *Methods Enzymol* **101**, 228-245 (1983).

50 D'Avino, P. P. *et al.* Interaction between Anillin and RacGAP50C connects the actomyosin contractile ring with spindle microtubules at the cell division site. *J Cell Sci* **121**, 1151-1158 (2008).
51 Zanin, E. *et al.* A conserved RhoGAP limits M phase contractility and coordinates with microtubule asters to confine RhoA during cytokinesis. *Dev Cell* **26**, 496-510, doi:10.1016/j.devcel.2013.08.005 (2013).
52 Guizetti, J. *et al.* Cortical constriction during abscission involves helices of ESCRT-III-dependent filaments. *Science* **331**, 1616-1620, doi:science.1201847 [pii] 10.1126/science.1201847 (2011).
53 Su, K. C., Takaki, T. & Petronczki, M. Targeting of the RhoGEF Ect2 to the equatorial membrane controls cleavage furrow formation during cytokinesis. *Dev Cell* **21**, 1104-1115, doi:S1534-5807(11)00513-2 [pii] 10.1016/j.devcel.2011.11.003 (2011).
54 Maliga, Z. *et al.* A genomic toolkit to investigate kinesin and myosin motor function in cells. *Nat Cell Biol* **15**, 325-334, doi:10.1038/ncb2689 (2013).
55 Hutterer, A., Glotzer, M. & Mishima, M. Clustering of centralspindlin is essential for its accumulation to the central spindle and the midbody. *Curr Biol* **19**, 2043-2049 (2009).
56 Poser, I. *et al.* BAC TransgeneOmics: a high-throughput method for exploration of protein function in mammals. *Nat Methods* **5**, 409-415, doi:10.1038/nmeth.1199 (2008).

Acknowledgments: We are very grateful to D.M. Glover for allowing us free access to his microscopy facility, to P.A. Coelho for help with time-lapse experiments and to Z. Lipinszki for helpful discussions. We thank D. Gerlich, A.A. Hyman, I. Poser, M. Petronczki, and E. Zanin for cell lines. This work was funded by a BBSRC grant (BB/R001227/1) to PPD.

Author contributions: Conceptualization: PPD, L. Capalbo and MM; Investigation: ZIB, L. Capalbo, PPD, MG, MED, ST, L. Copoiu, GC, MGR and LY; Formal analysis: ZIB, L. Capalbo, PPD, AE and EF; Funding acquisition: PPD; Methodology: ZIB, L. Capalbo and PPD; Project administration: PPD; Resources: JC, MED and MM; Supervision: PPD; Validation, ZIB, L. Capalbo and PPD; Visualization: ZIB, L. Capalbo, AE and PPD; Writing – original draft: PPD; Writing – review and editing: L. Capalbo, PPD, MG, JC, MM and SW.

Additional information. The authors declare no competing interests. Correspondence and requests for materials should be addressed to ppd21@cam.ac.uk.

Table 1.

Baits used in the AP-MS experiments for the characterization of the midbody interactome.

Name	Function	Localization	Tag and Cell Line Reference
Anillin	actomyosin binding protein; contractile ring scaffolding	cleavage furrow, midbody ring and secondary constriction sites	GFP[51]
Aurora B	serine/threonine kinase; CPC component, controls furrow ingression, central spindle formation and abscission	cleavage furrow, central spindle, midbody arms	GFP; (this study)
CHMP4B	ESCRT-III protein; required for abscission	midbody core and abscission site	GFP[52]
CHMP4C	ESCRT-III protein; required for abscission	central spindle, midbody arms, midbody core and abscission site	Flag[26]
Citron kinase (CIT-K)	serine/threonine kinase; required for midbody assembly, organization and maturation	cleavage furrow, central spindle, midbody ring	AcGFP[11]
Ect2	Rho GEF; activates RhoA to promote contractile ring assembly and constriction,	cleavage furrow, central spindle, midbody core	AcGFP[53]
KIF14	kinesin, CIT-K partner; required for midbody assembly, organization and maturation	cleavage furrow, central spindle, midbody ring	GFP[54]
KIF20A/MKLP2	kinesin; required for central spindle formation and CPC translocation	central spindle, midbody arms	GFP[54]
KIF23/MKLP1	kinesin; centralspindlin component, required for furrow ingression, central spindle and midbody formation	central spindle, midbody core	GFP[55]
PRC1	microtubule associated protein, required for central spindle and midbody formation	central spindle, internal midbody arms and core	GFP[56]

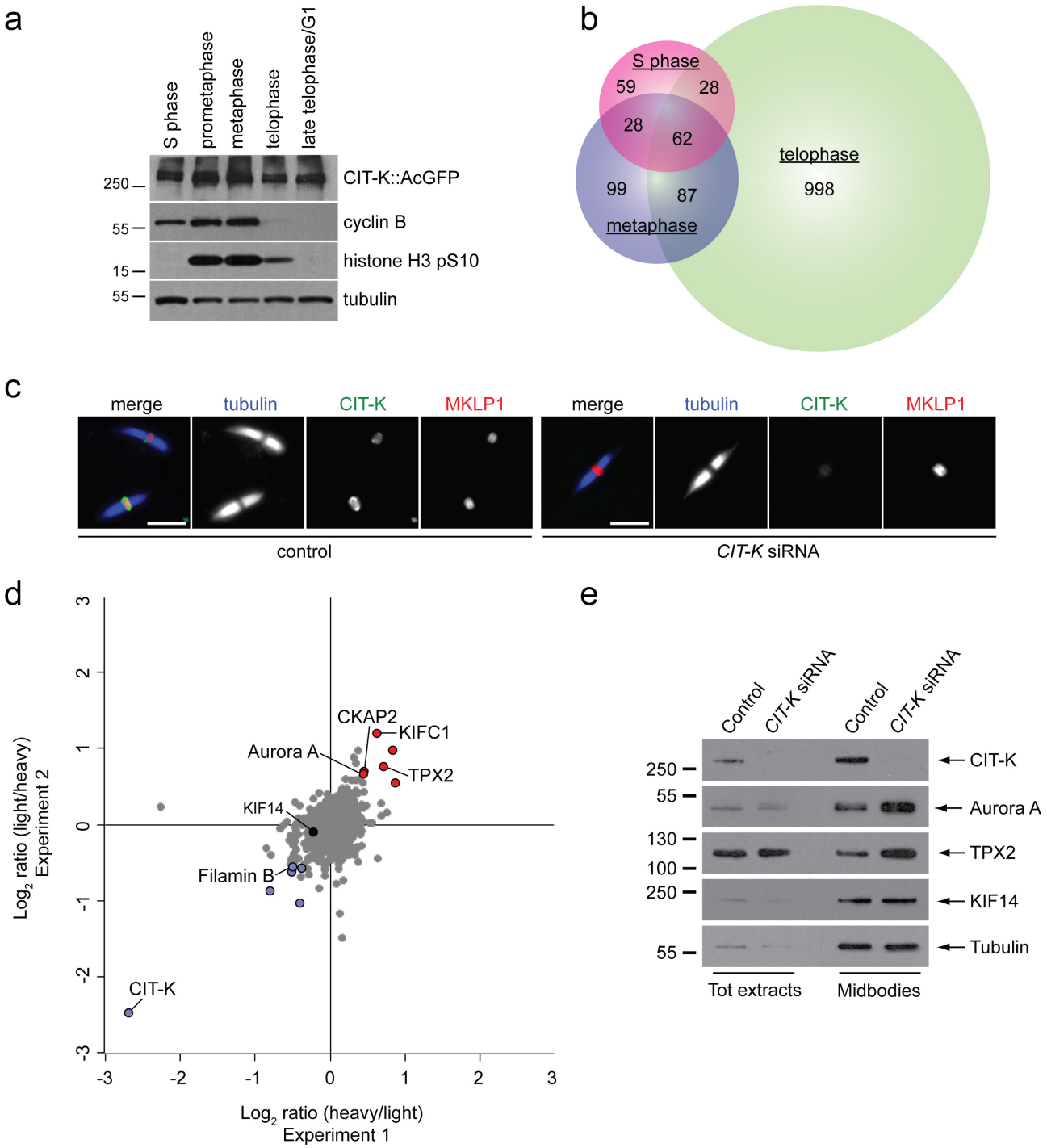

Fig. 1. CIT-K specifically interacts with a multitude of proteins in cytokinesis, but is not required for their recruitment to the midbody. (a) Western blot analysis of protein extracts from HeLa cells stably expressing a CIT-K::AcGFP transgene synchronized at different stages of the cell cycle. The blots were probed with antibodies against the proteins indicated to the right. Numbers on the left indicate the size, in kDa, of the protein ladder. (b) Proportional Venn diagram showing the number of proteins identified at each cell cycle stage by AP-MS using CIT-K::AcGFP as bait. (c) Midbodies purified from HeLa S3 cells treated with siRNAs directed against either a random sequence (control) or *CIT-K* were fixed and stained to detect tubulin, CIT-K and MKLP1. Scale bars, 5 µm. (d) Logarithmic normalized protein ratios from two independent SILAC experiments were plotted against each other. Each point represents a single protein identified. Gray dots correspond to proteins that did not show any significant difference in abundance between control and CIT-K siRNA midbodies. Red and blue dots represent proteins that were either significantly enriched or less abundant after CIT-

K depletion in both biological replicates (*p* value < 0.01). (e) Western blot analysis of total protein extracts and midbodies purified from telophase HeLa S3 cells treated with siRNAs directed against either a random sequence (control) or *CIT-K*. The blots were probed with antibodies against the proteins indicated to the right. Numbers on the left indicate the size, in kDa, of the protein ladder.

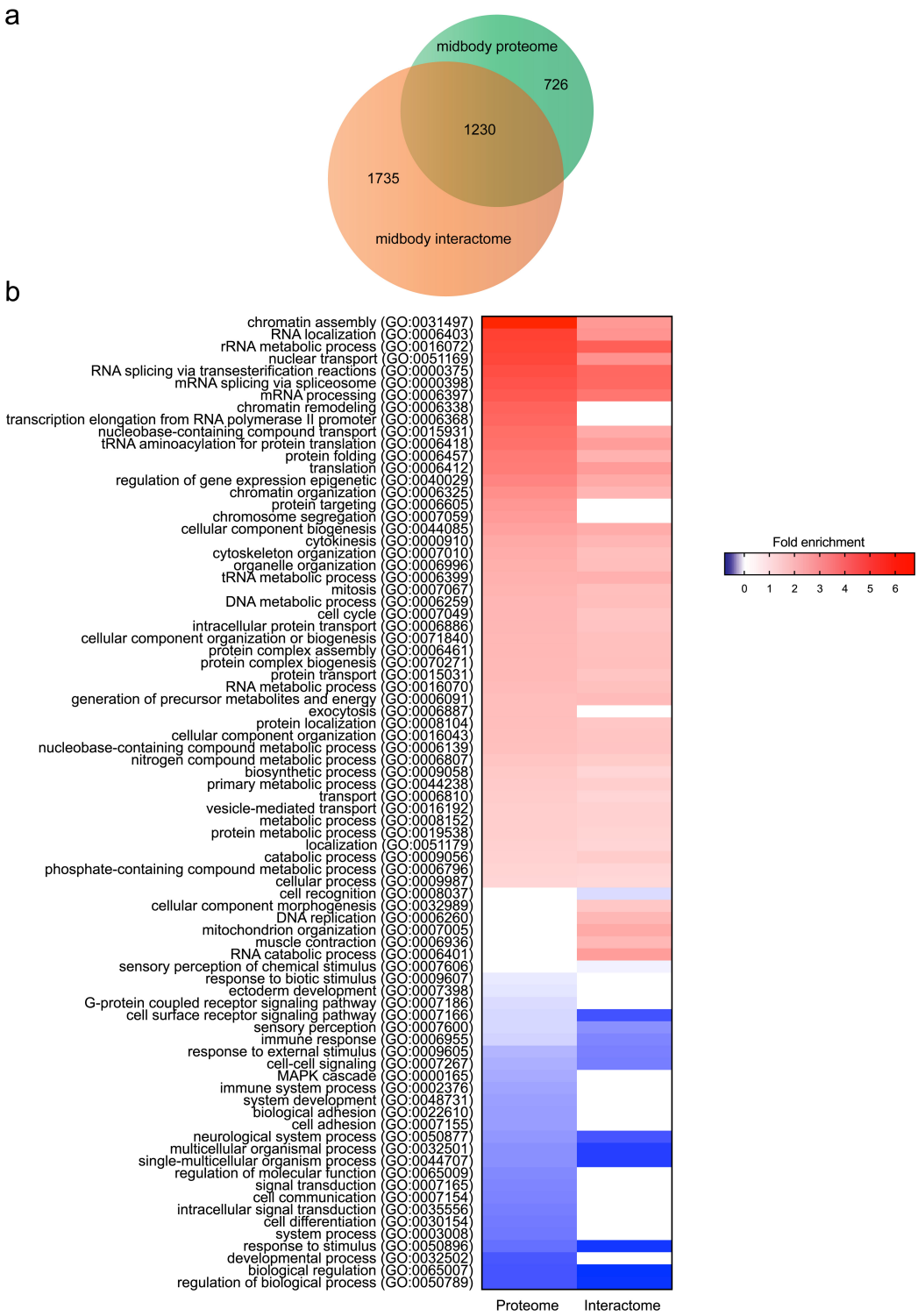

Fig. 2. The midbody proteome and the midbody interactome share many proteins and have similar Gene Ontology (GO) enrichment profiles. (a) Proportional Venn diagram showing the number of proteins identified in the midbody proteome and interactome. The majority of midbody proteome proteins (62.9%) are contained in the midbody interactome. (b) Heat map showing the GO annotation enrichment profiles of the midbody proteome and of the midbody interactome. GO enrichment profiles were analyzed using PANTHER under the category "GO-slim biological process". Overrepresented GO terms are shown in shades of red while underrepresented GO terms are shown in shades of blue, according to their fold enrichment. Only results for Bonferroni-corrected for $p < 0.05$ were considered (see Supplementary Data S5).

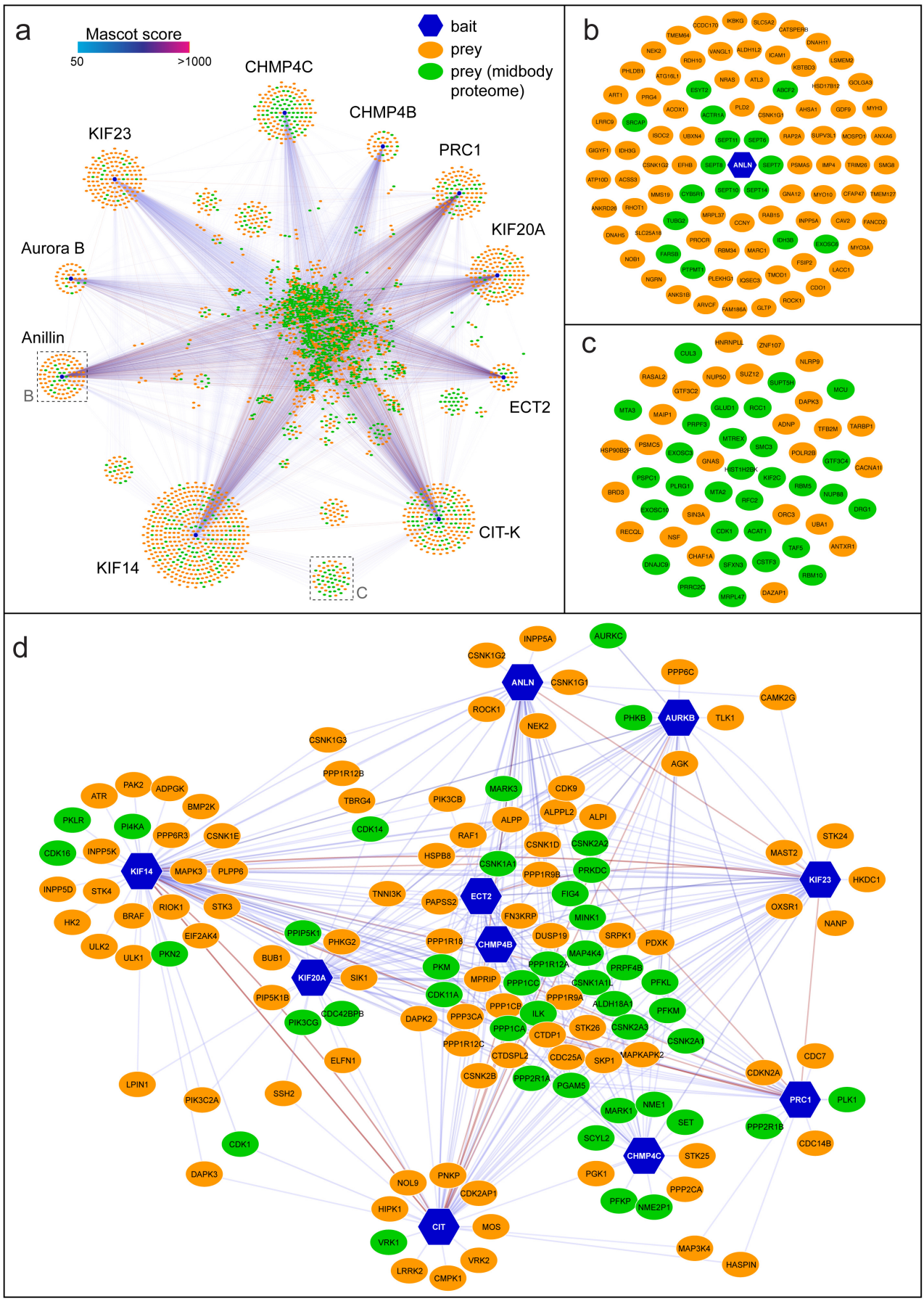

Fig. 3. The midbody interactome comprises common and specific networks. (a) Diagram illustrating the entire midbody interactome. Baits are indicated with blue hexagons, while preys are

represented as ovals, either in green, if they were also found in the midbody proteome, or in orange. The edges connecting the network nodes are colored according to their Mascot scores as indicated at the top left. Preys shared by multiple baits are clustered in the center. (b) Enlargement of the Anillin-specific sub-network shown in the corresponding inset in (a). (c) Enlargement of the baits shared specifically by CIT-K and KIF4 shown in the corresponding inset in (a). (d) Diagram representing the phosphorylation sub-network. All nodes are labelled with their primary gene names according to the UniProt database (https://www.uniprot.org).

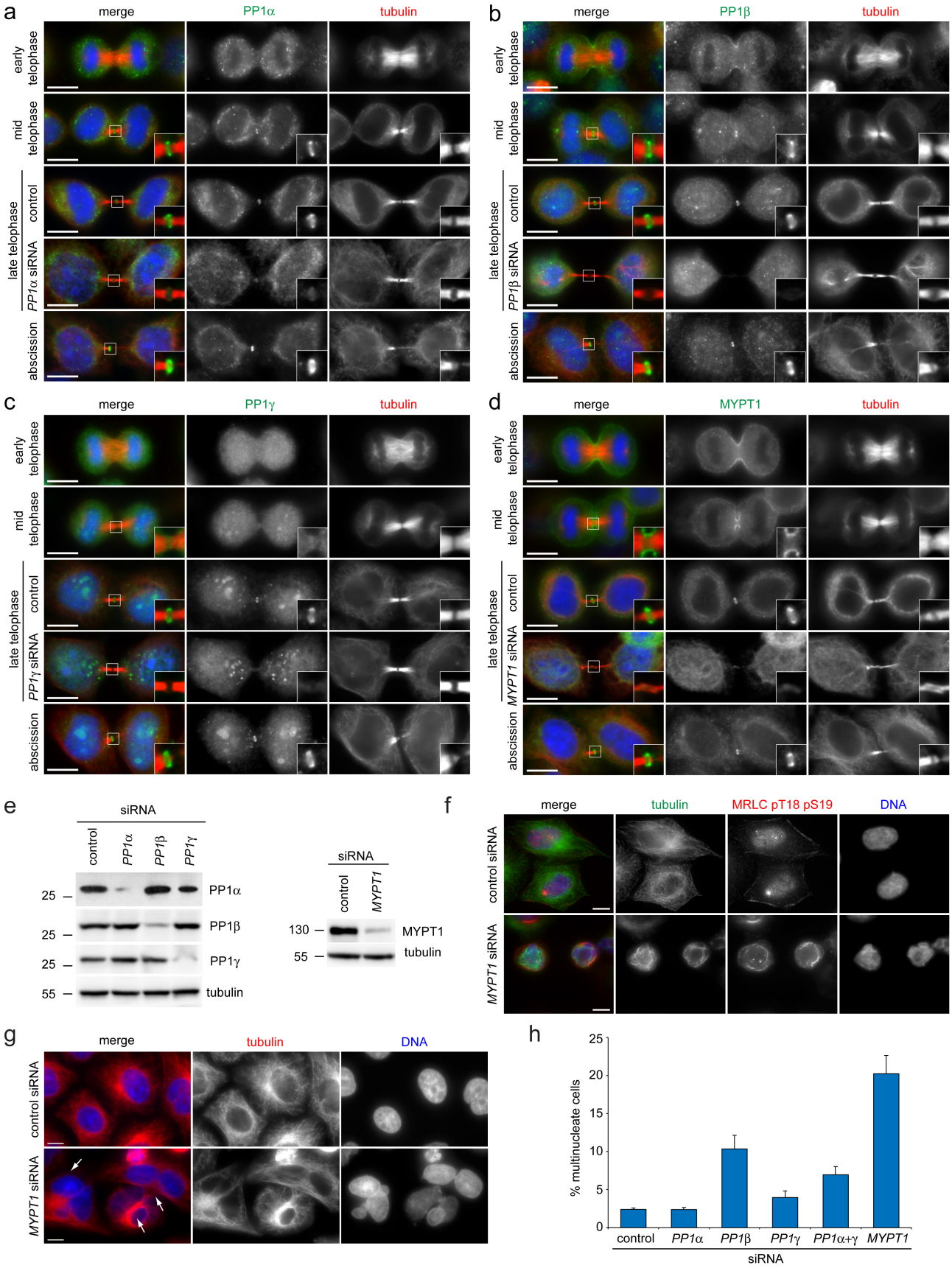

Fig. 4. PP1 phosphatases localize to the midbody and depletion of PP1β and MYPT1 causes cytokinesis failure. (a-d) HeLa cells were fixed and stained to detect to detect DNA (blue in the merged panels), tubulin, and PP1α (a) PP1β (b), PP1γ (c) and MYPT1 (d). For RNAi depletions, HeLa cells were treated with siRNAs directed against each of the three PP1 catalytic subunits or MYPT1

and after 48 hours were fixed and stained to detect the same epitopes as described above. DNA condensation and shape and thickness of microtubule bundles at the intercellular bridge were used as criteria to stage telophase cells. Insets show a 3x magnification of the midbody. Bars, 10 µm. (e) HeLa Kyoto cells were treated with siRNAs directed against either a random sequence (control) or each of the three PP1 catalytic subunits (left) or MYPT1 (right) and after 48 h proteins were extracted and analyzed by western blot to detect the indicated proteins. The numbers on the left indicate the sizes in kDa of the molecular mass marker. (f) HeLa cells were treated with siRNAs directed against either a random sequence (control) or *MYPT1* and after 48 hours were fixed and stained to detect DNA, tubulin and di-phosphorylated MRLC. Note that *MYPT1* siRNA cells show abnormal cell and nuclear shape and disorganized microtubule and actomyosin cytoskeletal filaments. Bars, 10 µm. (g) HeLa cells were treated with siRNAs directed against either a random sequence (control) or *MYPT1* and after 48 hours were fixed and stained to detect DNA and tubulin. The arrows indicate multinucleate cells. Bars, 10 µm. (h) Quantification of multinucleate cells obtained after siRNA of the three PP1 catalytic subunits or MYPT1. More than 500 cells were counted in each experiment, n=3. Bars indicate standard errors.

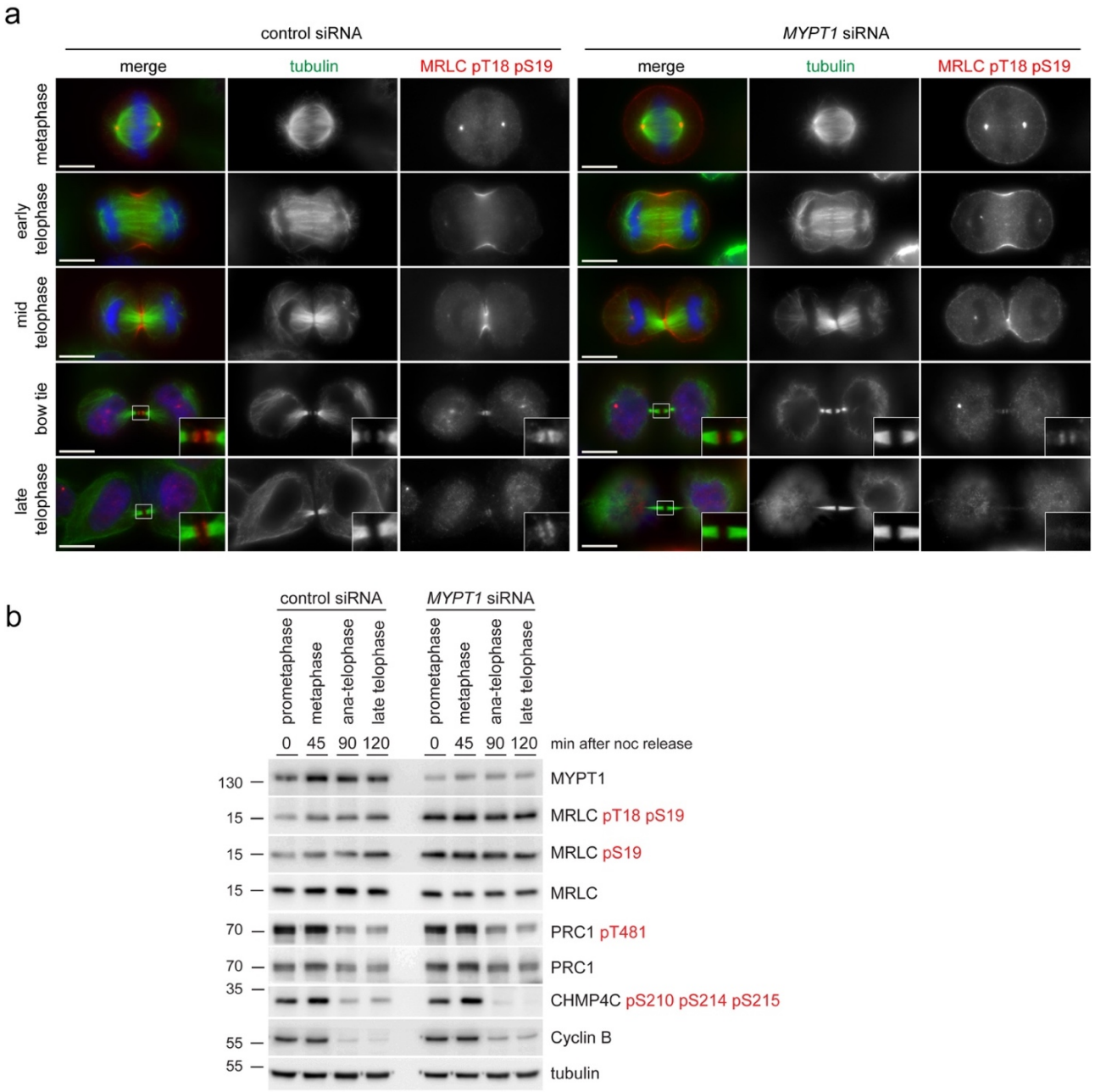

Fig. 5. ***MYPT1* siRNA increases the levels of phosphorylated MRLC, but does not impair furrow ingression and de-phosphorylation during mitotic exit.** (a) HeLa cells were treated with siRNAs directed against either a random sequence (control) or *MYPT1* and after 48 hours were fixed and stained to detect DNA (blue in the merged panels), tubulin and di-phosphorylated MRLC pT18 pS19. DNA condensation and the shape and thickness of microtubule bundles at the intercellular bridge were used as criteria to stage telophase cells. Insets show a 3x magnification of the midbody. Bars, 10 µm. (b) Time course analysis of protein expression and phosphorylation during mitotic exit after MYPT1 depletion. HeLa cells were treated with siRNAs directed against either a random sequence (control) or *MYPT1* and after 24 hours synchronized by thymidine/nocodazole block. Cells were collected at the indicate time points after nocodazole (noc) release and proteins extracted and used in Western blot analysis to identify the proteins and phospho-epitopes indicated to the right. The numbers on the left indicate the sizes of the molecular mass marker.

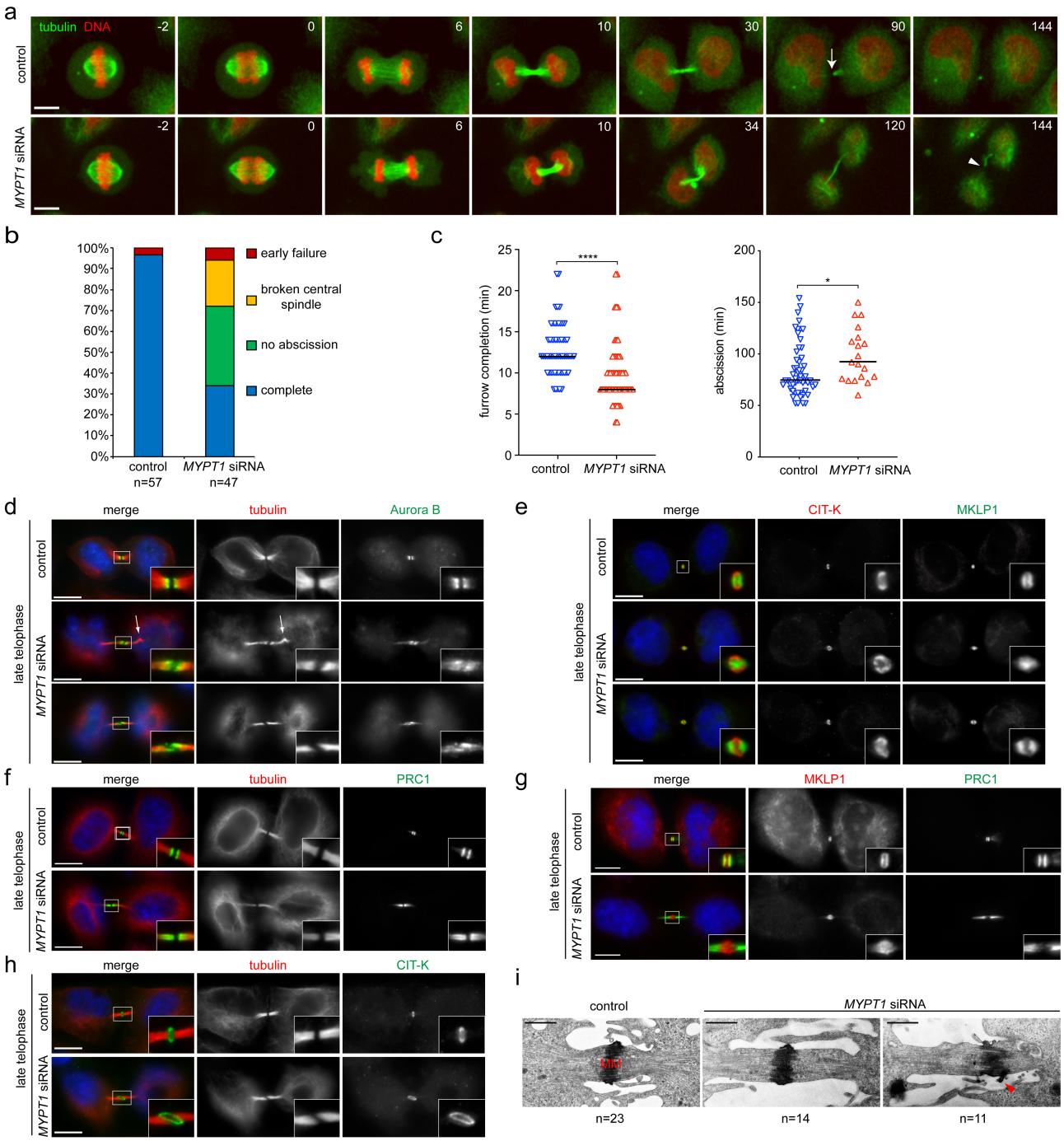

Fig. 6. MYPT1 is required for central spindle stability and midbody architecture. (a) Selected images from time-lapse recordings of HeLa Kyoto cells expressing GFP::tubulin and histone H2B::mCherry treated with siRNAs directed against either a random sequence (control) or *MYPT1* siRNA for 30 hours before filming. Time is in min relative to anaphase onset. The arrow in the 90 min control cell marks the abscission site, while the arrowhead in the 144 min *MYPT1* siRNA cell marks the rupture of the central spindle. Bar, 10 µm. (b) Graph showing the frequency of phenotypes observed in the time-lapse recordings described in (a). Categories: "no abscission" indicates cells that either failed abscission or failed to fully separate and were still connected by central spindle microtubules at the end of filming, which was more than 2 and up to 6 h (Supplementary Video S7); "early failure" indicates cells that failed to form a midbody and cleavage furrows collapsed (Supplementary Video S8); "broken central spindles" indicates cells in which the central spindle broke before abscission occurred, like in the cell shown in (a) and in Supplementary Video S6. (c) Scatter plots showing quantification of furrow ingression (from anaphase onset to

furrow completion; left) and abscission (from furrow completion to abscission; right) times measured in the time-lapse recordings described in (a). For *MYPT1* siRNA cells, abscission times were only measured from cells that successfully completed abscission (indicated by the blue bar in b). Horizontal bars indicate medians; **** $p < 0.0001$ (student's T-test); * $p < 0.01$ (Mann–Whitney *U* test). (d-h) HeLa Kyoto cells were treated with siRNAs directed against either a random sequence (control) or *MYPT1* siRNA and after 48 hours were fixed and stained to detect the indicated epitopes and DNA (blue in the merged panels). DNA condensation and the shape and thickness of microtubule bundles at the intercellular bridge were used as criteria to stage telophase cells. Insets show a 3x magnification of the midbody. The arrow in (d) marks a bend in the central spindle. Bars, 10 µm. (i) Electron micrographs of midbodies in HeLa cells treated with a siRNA directed against either a random sequence (control) or *MYPT1* for 48 hours. The arrowhead marks an abnormal protrusion of the midbody matrix (MM). Bars, 1 µm.

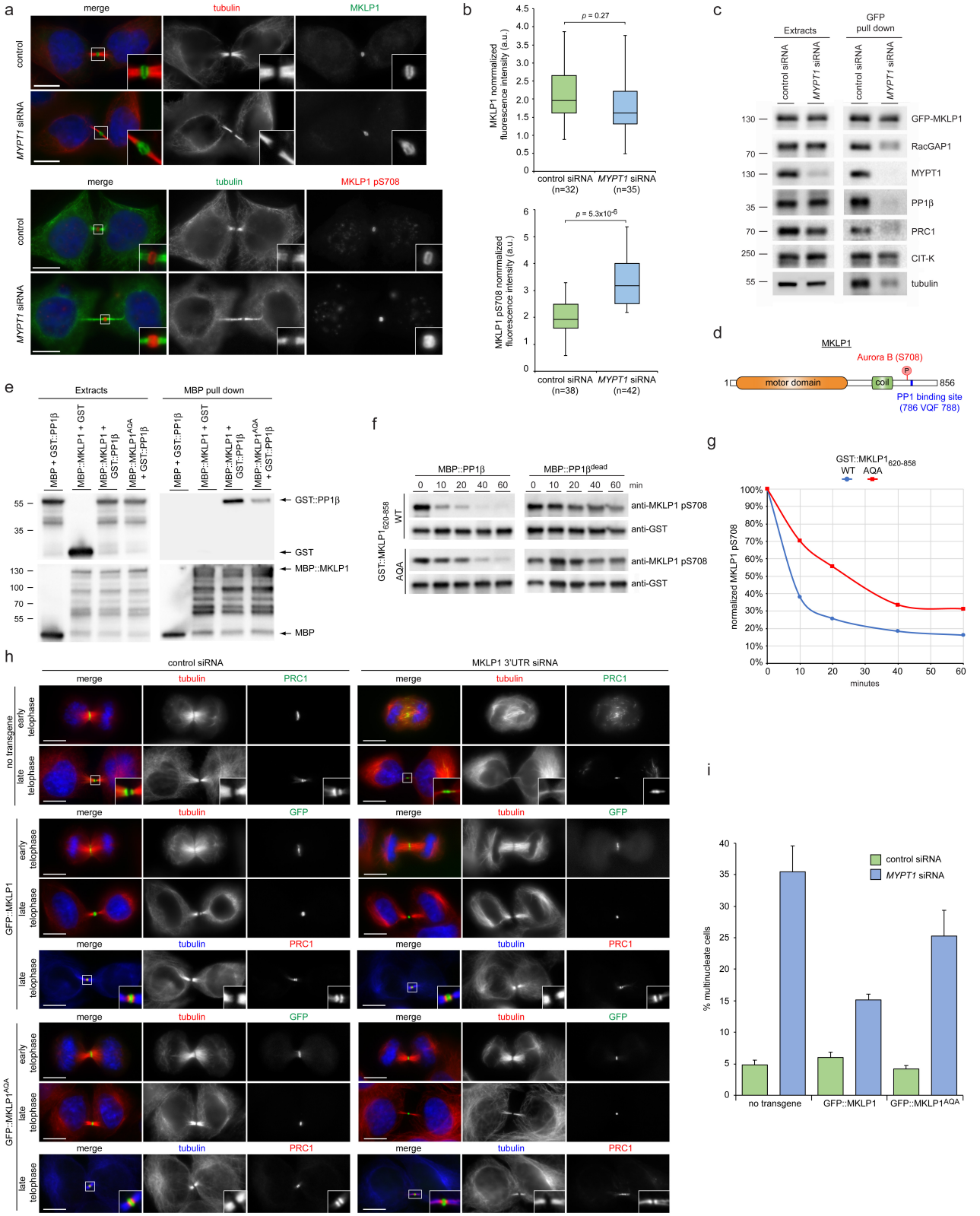

Fig. 7. MYPT1/PP1β de-phosphorylates MKLP1 at S708 in cytokinesis. (a) HeLa Kyoto cells were treated with siRNAs directed against either a random sequence (control) or *MYPT1* siRNA and after 48 hours fixed and stained to detect the indicated epitopes and DNA (blue in the merged panels). DNA condensation and the shape and thickness of microtubule bundles at the intercellular bridge were used as criteria to stage telophase cells. Insets show a 3x magnification of the midbody. Bars, 10 µm. (b) Box plots showing the quantification of total and pS708 MKLP1 in control and *MYPT1* siRNA late telophase cells. Fluorescence intensities of MKLP1 and MKLP1 pS708 were calculated as described in Methods. AU, arbitrary unit. The numbers of cells counted are indicated below each

plot. *p* values were calculated using the student's T-test. (c) HeLa Kyoto cells stably expressing GFP-MKLP1 were treated with either a random sequence (control) or *MYPT1* siRNA and after 24 hours synchronized in telophase by thymidine/nocodazole block. Protein extracts were used in a GFP pull-down assay and then extracts and pull-downs were analyzed by Western blot to detect the proteins indicated to the right. The numbers on the left indicate the sizes of the molecular mass marker. (d) Schematic diagram of the MKLP1 protein. The Aurora B phosphorylation site at S708 and the VQF PP1 binding site are indicated. (e) MBP-tagged MKLP1, MKLP1^{AQA} or MBP alone were co-expressed in yeast along with either GST alone or GST-PP1β as indicated at the top. Protein extracts were used in a pull-down assay using amylose beads. Crude extracts and pull-downs were analyzed by Western blot to detect GST (top panels) and MBP (bottom panels). Numbers on the left indicate the size, in kDa, of the protein ladder. (f) GST-tagged wild type and AQA mutant MKLP1 fragments (aa 620-858) were expressed and purified in bacteria and then phosphorylated *in vitro* with recombinant Aurora B. After washing out Aurora B, the reactions were incubated with either MBP-tagged PP1β or a catalytically dead version (PP1β^{dead}) purified from yeast for the times indicated at the top. Proteins were then analyzed by Western blot using antibodies against MKLP1 pS708 and GST. (g) Graph showing the quantification of MKLP1 pS708 values normalized against the total amounts of GST-MKLP1$_{620-858}$. (h) HeLa Kyoto cells stably expressing GFP-MKLP1, GFP-MKLP1^{AQA} or no transgene, were treated with either a random sequence (control) or an siRNA targeted against the *MKLP1* 3'UTR region, which is not present in the GFP-tagged MKLP1 transgenes, and after 48 hours were fixed and stained to detect the indicated epitopes and DNA (blue in the merged panels). DNA condensation and the shape and thickness of microtubule bundles at the intercellular bridge were used as criteria to stage telophase cells. Bars, 10 µm. (i) Quantification of multinucleate cells, a readout for cytokinesis failure, from the experiments shown in (h). More than 500 cells were counted in each experiment, n=3. Bars indicate standard errors.

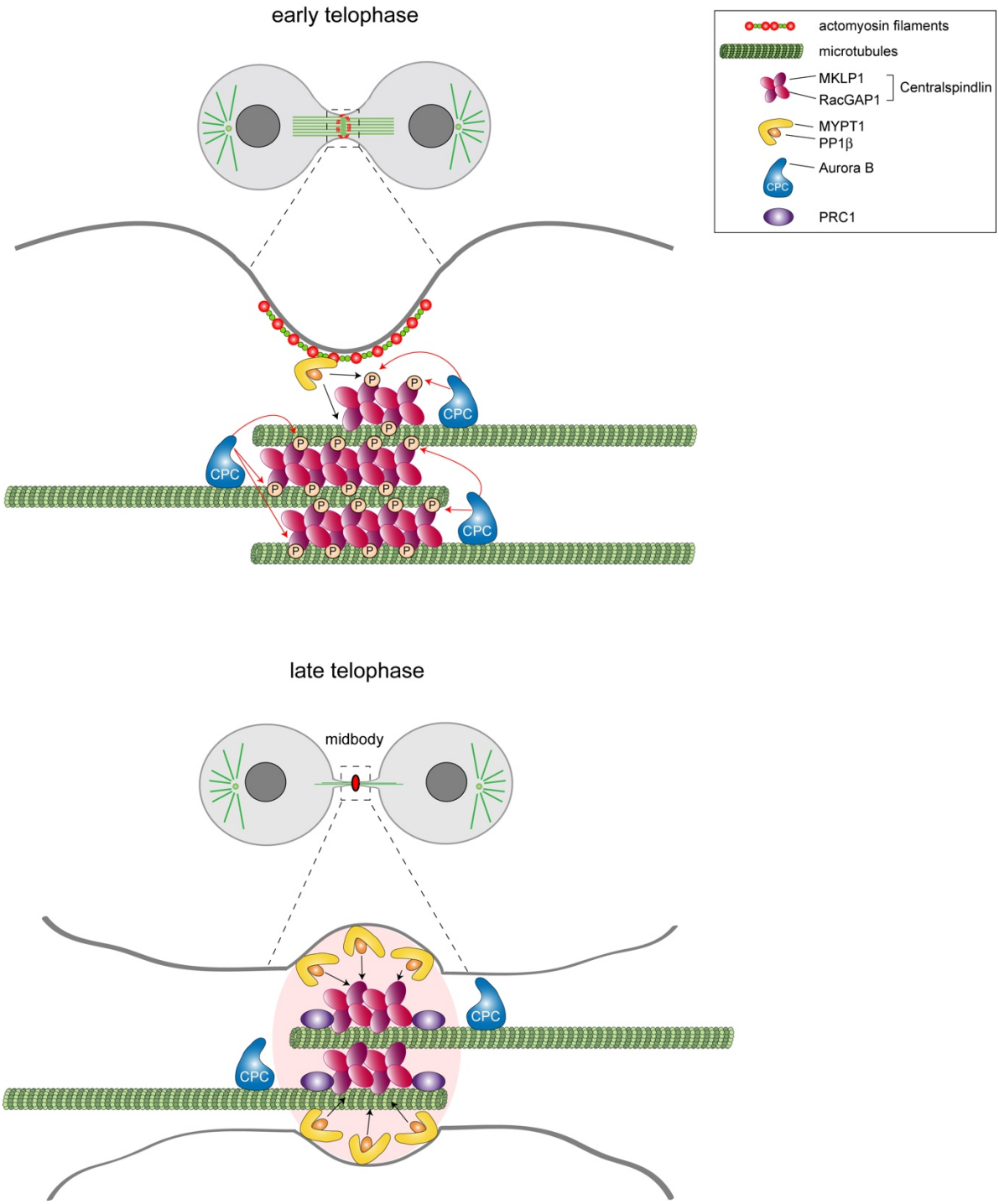

Fig. 8. Model illustrating how different distribution of Aurora B and MYPT1-PP1β can regulate centralspindlin activity at different stages during cytokinesis. During furrowing (top panel) MYPT1-PP1β accumulates at the cortex with no or very limited access to the centralspindlin pool that localizes to the central spindle midzone, which is highly phosphorylated by Aurora B and therefore can form clusters. After completion of furrow ingression, MYPT1/PP1β accumulates at the midbody ring whereas Aurora B localizes to the midbody arms (bottom panel). This allows PP1β to de-phosphorylate MKLP1 at S708, which could strengthen the association of centralspindlin with PRC1. See text for more details.